Linear response theory for detectors consisting of discrete arrays

Michael Albert and Andrew D. A. Maidment

Linear response theory for detectors consisting of discrete arrays

Michael Albert and Andrew D. A. Maidment[a]
Thomas Jefferson University, Department of Radiology, Suite 3390, Gibbon Building,
111 South 11th Street, Philadelphia, Pennsylvania 19107-5563

The optical transfer function (OTF) and the noise power or Wiener spectrum are defined for detectors consisting of a lattice of discrete elements with the assumptions of linear response, Gaussian statistics, and stationarity under the discrete group of translations which leave the lattice fixed. For the idealized classification task of determining the presence or absence of a signal under signal known exactly/background known exactly (SKE/BKE) conditions, the Wiener spectrum, the OTF, along with an analog of the gray-scale transfer characteristic, determine the signal-to-noise ratio (SNR), which quantifies the ability of an ideal observer to perform this task. While this result is similar to the established result for continuous detectors, such as screen-film systems, the theory of discrete lattices of detectors must take into account the fact that the lattice only supports a bounded but (in the limit of a detector of arbitrarily great extent) continuous range of frequencies. Incident signals with higher spatial frequencies appear in the data at lower aliased frequencies, and there are pairs of signals which are not distinguishable by the detector (the SNR vanishes for the task of distinguishing such signals). Further, the SNR will in general change if the signal is spatially displaced by a fraction of the lattice spacing, although this change will be small for objects larger than a single pixel. Some of the trade-offs involved in detectors of this sort, particularly in dealing with signal frequencies above those supported by the lattice, are studied in a simple model. © *2000 American Association of Physicists in Medicine.* [S0094-2405(00)00908-1]

I. INTRODUCTION

The importance of signal detection theory in quantifying the performance of medical imaging systems (x-ray screen-film imaging being perhaps the best example) gives impetus to applying the same techniques to the digital radiographic imaging systems which are now coming into clinical use. As applied to screen-film systems, signal detection theory requires three assumptions to be at least approximately fulfilled: that the detector responds linearly to the incoming signal, and is both stationary and homogeneous (i.e., both the detector response and the additive noise are translationally invariant). One can then summarize the response of the system in terms of the gray-scale transfer characteristic, the optical transfer function (OTF), and the noise power or Wiener spectrum.

The digital x-ray imaging systems which are now appearing generally behave as a lattice of discrete detector elements. Although digital, these detectors are generally operated under conditions such that the effects of quantization are negligible. When compared to screen-film systems, these detectors tend to be linear over a wider range of exposures. Like screen-film, for low-contrast signals the noise is approximately additive and Gaussian. However, as the size of the imaging elements is now comparable to the size of some of the smaller objects which are of clinical interest (around 0.1 mm), these detectors are not strictly homogeneous in that translations by a fraction of the lattice spacing result in the signal being recorded in a different manner. As these devices generally consist of a regular lattice of sensitive elements, they still possess a symmetry with respect to a discrete group of translations. This symmetry is approximate due to the finite extent of physical detectors. However, as in the theory of screen-film systems, corrections for the limited extent of the detector are negligible for many practical applications. Thus, one can apply Fourier techniques to put the signal detection theory of such devices in a form which is both tractable and similar to the theory of screen-film systems. Instead of using a continuous Fourier transform, one uses a discrete space Fourier transform, which recodes the data acquired by the detector at a discrete lattice of positions in terms of a bounded and continuous range of spatial frequencies.

For screen-film systems, the OTF diagonalizes the linear operator which relates the input signal to the output. As detailed below, for discrete-array detectors the effects of aliasing introduce a null space, different for each device, which prevents this operator from being diagonalized using a basis common to all devices, but the OTF represents the operator in a basis in which it is sparse in the sense that all terms vanish except those between input and output spatial frequencies which are equal or aliased. The Wiener spectrum is the discrete space Fourier transform of the discrete autocovariance function, and thus is also defined in the region of frequency space which the lattice supports. As in the case of continuous detectors, for low-contrast objects (so that responses are approximately linear), these quantities determine the signal-to-noise ratio (SNR) which is an appropriate figure-of-merit for the classification task of discriminating between the presence or absence of an exactly known signal against an exactly known background (SKE/BKE).

To make notation definite, it is necessary to review the relevant parts of signal detection theory for screen-film imaging systems (Sec. II) and the relevant Fourier techniques (Sec. III). Subsequently, the OTF (Sec. IV) and Wiener spectrum (Sec. V) of discrete detectors can be studied leading up to the calculation of SNR for the case of SKE/BKE (Sec. VI).

As discussed below, the effects of aliasing on the interpretation of the OTF have been noted in the literature, and the definition of the Wiener spectrum given here has appeared before. However, this paper presents a systematic theory of signal detection for discrete-array x-ray detectors. The approach here differs from the more general theoretical approach of cross-talk matrices[1] in that the work reported here uses the additional assumptions of infinite extent, Gaussian statistics, and discrete translational symmetry. There are many imaging systems for which these assumptions are not appropriate [e.g., three-dimensional (3D) tomographic reconstruction[2]). However, the work presented here has certain advantages in that so long as the additional assumptions are approximately true, the quantities involved are closely related to those used with screen-film systems and are similar or identical to measured quantities relating to digital systems which have appeared in the literature.

To demonstrate the use of this theoretical structure and to investigate some of the trade-offs inherent in discrete-array systems, Sec. VII presents a simple model of a detector. In particular, this gives the opportunity to investigate how the detector's response to high spatial-frequency signals affects the detection of objects in terms of SNR, and in particular the effect which is sometimes called ''noise aliasing'' is addressed.

II. REVIEW

The theory of SKE/BKE detection and classification for screen-film-like systems has been expounded in detail,[3–7] and is reviewed here in order to establish notation for later comparison with discrete-array detectors. The input signal is the x-ray intensity per unit area and the output signal is the film density, both as a function of position. The interesting and tractable case is the search for low-contrast variations $I(\mathbf{r})$ in an x-ray beam whose baseline intensity, I_o, is such that the changes in film density $D(\mathbf{r})$ are a linear function of $I(\mathbf{r})$. The additional assumption of translational invariance then gives

$$\langle D(\mathbf{r})\rangle=\frac{\gamma(\log_{10}e)}{I_o}\int\int d^2\mathbf{r}'\,P(\mathbf{r}-\mathbf{r}')\langle I(\mathbf{r}')\rangle,\qquad(1)$$

where $P(\mathbf{r}-\mathbf{r}')$, the point spread function (PSF), is the density increase of the film at position $\mathbf{r}$ due to a given x-ray intensity at $\mathbf{r}'$. The brackets $(\langle\rangle)$ represent ensemble averages, i.e., averages over many exposures. Since $I(\mathbf{r})$ and $D(\mathbf{r})$ are here defined as variations relative to baseline values, $\langle I(\mathbf{r})\rangle=0$ and $\langle D(\mathbf{r})\rangle=0$ in the absence of a signal.

Because the PSF is translationally invariant, the convolution operator is diagonalized in frequency space, giving

$$\langle\hat{D}(\mathbf{f})\rangle=\frac{\gamma(\log_{10}e)}{I_o}\,T(\mathbf{f})\langle\hat{I}(\mathbf{f})\rangle,\qquad(2)$$

where $\mathbf{f}$ represents a two-dimensional vector in frequency space and T, the optical transfer function (OTF), is the Fourier transform of the PSF. The function $\hat{D}(\mathbf{f})$ is the Fourier transform of the data $D(\mathbf{r})$, following the convention that for any suitable[8] function g,

$$\hat{g}(\mathbf{f})=\int\int d^2\mathbf{r}\,g(\mathbf{r})e^{-2\pi i\mathbf{r}\cdot\mathbf{f}},$$

$$g(\mathbf{r})=\int\int d^2\mathbf{f}\,\hat{g}(\mathbf{f})e^{2\pi i\mathbf{r}\cdot\mathbf{f}},\qquad(3)$$

so that $\mathbf{f}$ is in units of cycles per unit length. The factor of $\gamma(\log_{10}e)/I_o$ serves to convert units of x-ray beam intensity into units of change of film density in the region of linear response, allowing the normalization $T(\mathbf{0})=1$.

Realizations of the imaging process will be subject to noise which can be characterized by the autocovariance function

$$C(\mathbf{r}_1,\mathbf{r}_2)=C(\mathbf{r}_2,\mathbf{r}_1)=\langle D(\mathbf{r}_1)D(\mathbf{r}_2)\rangle,\qquad(4)$$

that, for Gaussian noise, completely determines the statistical nature of the noise process. For stationary processes, the autocovariance function depends only upon the displacement,

$$C(\mathbf{r}_1,\mathbf{r}_2)=C(\mathbf{r}_2-\mathbf{r}_1),\qquad(5)$$

so that the autocovariance $C(\mathbf{r})$ is now a function of a single vector, the displacement $\mathbf{r}$. The Wiener spectrum is the Fourier transform of the autocovariance function, and

$$W(\mathbf{f})=\lim_{|A|\to\infty}\frac{1}{|A|}\left\langle\left|\int\int_A d^2\mathbf{r}D(\mathbf{r})e^{-2\pi i\mathbf{r}\cdot\mathbf{f}}\right|^2\right\rangle\qquad(6)$$

shows that the Wiener spectrum can be estimated in terms of the Fourier components of signal-free (''flat-field'') images over regions A of sufficiently large area $|A|$.

For Gaussian noise it can be shown[9] that the optimal strategy for SKE/BKE signal detection or classification consists of choosing a mask function $g(\mathbf{r})$ and a cutoff value for the statistic

$$\theta_g=\int\int d^2\mathbf{r}g(\mathbf{r})D(\mathbf{r}).\qquad(7)$$

The efficacy of θ_g for discriminating between hypothesis I (e.g., signal absent) and hypothesis II (e.g., signal present) is measured by the signal-to-noise ratio

$$\text{SNR}_g^2=\frac{(\langle\theta_g\rangle_\text{I}-\langle\theta_g\rangle_\text{II})^2}{\text{Var}(\theta_g)},\qquad(8)$$

where the numerator is the difference between the expectation values of θ_g under the two hypotheses and the denominator is the variance in the statistic θ_g, which for additive noise is independent of the hypothesis.

While only real-valued functions $g(\mathbf{r})$ are needed for calculating decision statistics, it will be useful to extend the definition of θ_g to complex valued $g(\mathbf{r})$, in which

case the variance of θ_g is the sum of the variances of the real and imaginary parts. The variance of the statistic θ_g is given by

$$\text{Var}(\theta_g) = \langle (\theta_g - \langle \theta_g \rangle)(\theta_g - \langle \theta_g \rangle)^* \rangle \tag{9}$$

$$= \int \int d^2\mathbf{r} \int \int d^2\mathbf{r}' g(\mathbf{r}) C(\mathbf{r}, \mathbf{r}') g(\mathbf{r}')^* \tag{10}$$

$$= \int \int d^2\mathbf{f} \hat{g}(\mathbf{f}) \hat{g}^*(\mathbf{f}) W(\mathbf{f}), \tag{11}$$

as can be seen by substitution of Eqs. (7) and (4) into Eq. (9) [indeed, Eq. (10) can be taken as the definition of the auto-covariance function]. It can be shown, for example using the Schwarz inequality,[10,11] that the optimal choice of mask function is given by

$$\hat{g}_{\mathcal{I}}(\mathbf{f}) = \frac{(\langle \hat{I}(\mathbf{f}) \rangle_{\text{II}} - \langle \hat{I}(\mathbf{f}) \rangle_{\text{I}}) T(\mathbf{f})}{W(\mathbf{f})}, \tag{12}$$

for which the SNR is given by

$$\text{SNR}_{\mathcal{I}}^2 = \int \int d^2\mathbf{f} \frac{\gamma^2 (\log_{10} e)^2}{I_o^2} \frac{|\langle \hat{I}(\mathbf{f}) \rangle_{\text{II}} - \langle \hat{I}(\mathbf{f}) \rangle_{\text{I}}|^2 |T(\mathbf{f})|^2}{W(\mathbf{f})}, \tag{13}$$

where the subscript $\mathcal{I}$ indicates that this represents the optimal or ideal[7] observer given the detector and task at hand.

Returning momentarily to the task of estimating the Wiener spectrum from flat-field images, if in Eq. (9) one sets $g(\mathbf{r}) = G(\mathbf{r}) e^{2\pi i \mathbf{f}_o \cdot \mathbf{r}}$, where $G(\mathbf{r})$ is a window function with normalization

$$\int \int d^2\mathbf{r} G^2(\mathbf{r}) = 1, \quad \int \int d^2\mathbf{f} |\hat{G}(\mathbf{f})|^2 = 1, \tag{14}$$

then calculating $\langle \theta_g \theta_g^* \rangle$ by Eq. (11) one obtains

$$\int \int d^2\mathbf{f} |\hat{G}(\mathbf{f} - \mathbf{f}_o)|^2 W(\mathbf{f})$$

$$= \left\langle \left| \int \int d^2\mathbf{r} G(\mathbf{r}) e^{-2\pi i \mathbf{f}_o \cdot \mathbf{r}} D(\mathbf{r}) \right|^2 \right\rangle, \tag{15}$$

which, since $|\hat{G}(\mathbf{f} - \mathbf{f}_o)|^2$ will be sharply peaked near $\mathbf{f}_o$, shows that for finite length data sets one actually estimates the Wiener spectrum convolved with the square of the Fourier transform of the window function. In particular, for a rect window so that G is chosen to vanish outside of a square region of area $|A| = L^2$ and to have value $1/\sqrt{|A|}$ inside that region,

$$|\hat{G}(\mathbf{f})|^2 = A \left(\frac{\sin(\pi L f_x) \sin(\pi L f_y)}{\pi^2 L^2 f_x f_y} \right)^2$$

$$= A \, \text{sinc}^2(L f_x) \text{sinc}^2(L f_y), \tag{16}$$

where f_x, f_y are the components of $\mathbf{f}$. For large areas, this becomes increasingly like a delta-function, giving Eq. (6).

III. MATHEMATICAL PRELIMINARIES

In the case of screen-film, described above, we studied a mapping of functions defined for all spatial positions to func-

tions defined for all frequencies, namely the Fourier transform defined by Eq. (3). For the digital x-ray detectors of interest in this paper, the input is still a continuous distribution of x-rays, but the output signal consists of data with values assigned only at a discrete set of lattice points. The size of the array is assumed to be sufficiently large so that boundary effects play no part, and thus is treated as being of infinite extent. To analyze these data it is appropriate to use a Fourier technique based on the discrete translational symmetry of the detectors. Mathematically, this transform is similar to the Fourier series, but with the roles of the space and frequency domains reversed.[12] Following Giger,[13] this is called the ''discrete'' space Fourier transform (DFT). The ''finite'' Fourier transform (FFT)[14] is the Fourier technique applied to finite sequences of data points that is customarily implemented using an algorithm known as the ''fast Fourier transform.'' For practical purposes, one always deals with finite data sets, and the discrete space Fourier transform is a limiting case of the finite Fourier transform. As the number of equally spaced data points used in calculating a finite Fourier transform increases, the discrete set of frequencies calculated fill more and more densely a bounded region of frequency space, so that in the limit one obtains a function of a continuous range of frequencies. The function obtained by this limiting process is the discrete space Fourier transform of the spatial data.

To deal with the two-dimensional arrangements of sensitive elements which are of interest, it will be convenient to introduce the ideas of vectors generating a lattice and of dual basis vectors. A two-dimensional lattice of points can be specified by vectors $\mathbf{v}_1$ and $\mathbf{v}_2$ such that every point in the lattice can be represented as

$$\mathbf{r}_{m_1, m_2} = m_1 \mathbf{v}_1 + m_2 \mathbf{v}_2, \tag{17}$$

where m_1 and m_2 are integers. The vectors $\mathbf{v}_1$ and $\mathbf{v}_2$ are said to generate the lattice, but the choice of vectors for a given lattice is not unique. For the common case of a square grid the choice of $\mathbf{v}_1$ as lying along the x-axis and $\mathbf{v}_2$ as lying along the y-axis is natural. The plane containing the lattice can be tiled in such a way that each tile contains a total of one lattice point. Each tile is then called a ''unit cell.'' For the case of a square grid of detectors with spacing a, the most natural choice of a unit cell would be the square centered at the coordinate origin extending to $\pm a/2$ along both axes. A small region of a plane containing a square lattice and one of the unit cells is drawn in Fig. 1(a). The reciprocal vectors denoted by $\mathbf{w}_1$ and $\mathbf{w}_2$ are defined by the requirements

$$\mathbf{v}_i \cdot \mathbf{w}_j = \delta_{ij} = \begin{cases} 1 : i = j \\ 0 : i \neq j \end{cases}, \tag{18}$$

and serve as a basis for frequency space and as generators of the reciprocal lattice. In the case of the rectangular grid mentioned above, each $\mathbf{w}_i$ would be parallel to $\mathbf{v}_i$ and scaled appropriately as illustrated in Fig. 1(b), which also shows a unit cell of the reciprocal lattice. To help clarify these ideas, Fig. 1(c) shows a hexagonal lattice with two choices of the
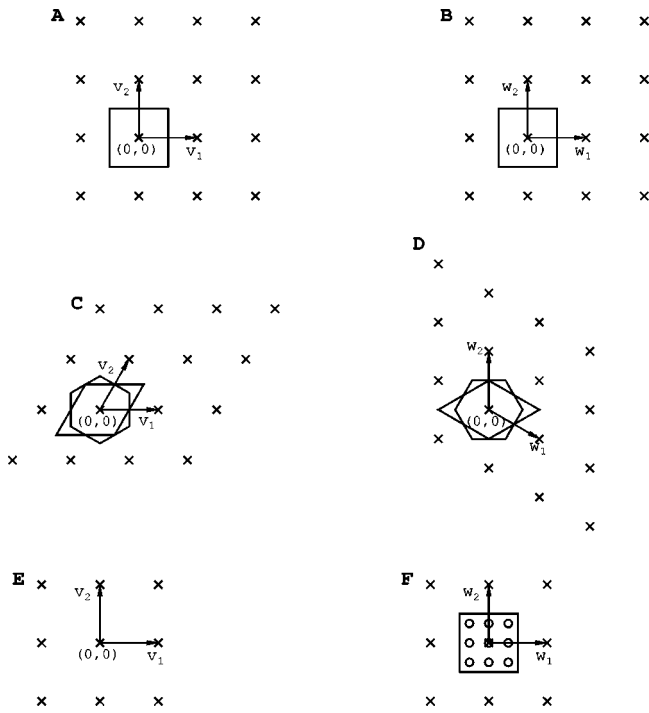
FIG. 1. (a) a rectangular lattice. (b) The reciprocal lattice of (a). (c) A hexagonal lattice. (d) the reciprocal lattice of (c). Note that (a), (b), (c), and (d) represent a finite region of a lattice which covers the entire plane. (e) A 3×3 finite rectangular lattice. (f) The circles represent the frequencies used in the finite Fourier transform of (e). For comparison, a unit cell of the full reciprocal lattice is shown. See Sec. III for details.

unit cell (parallelogram or hexagon) and Fig. 1(d) shows the reciprocal lattice (note that $\mathbf{v}_1$ is perpendicular to $\mathbf{w}_2$ and $\mathbf{v}_2$ is perpendicular to $\mathbf{w}_1$). The area $|A|=|\mathbf{v}_1\times\mathbf{v}_2|$ of a unit cell is independent of the choice of unit cell, since it is fixed by the average density of lattice points over large regions. The area of the unit cell of the reciprocal lattice, $|K|=|\mathbf{w}_1\times\mathbf{w}_2|$, is inversely proportional to $|A|$, as can be seen by

$$|A||K|=\left|\det\begin{pmatrix}(\mathbf{v}_1)_x & (\mathbf{v}_1)_y \\ (\mathbf{v}_2)_x & (\mathbf{v}_2)_y\end{pmatrix}\det\begin{pmatrix}(\mathbf{w}_1)_x & (\mathbf{w}_2)_x \\ (\mathbf{w}_1)_y & (\mathbf{w}_2)_y\end{pmatrix}\right| \quad (19)$$

$$=\left|\det\begin{pmatrix}\mathbf{v}_1\cdot\mathbf{w}_1 & \mathbf{v}_1\cdot\mathbf{w}_2 \\ \mathbf{v}_2\cdot\mathbf{w}_1 & \mathbf{v}_2\cdot\mathbf{w}_2\end{pmatrix}\right|$$

$$=\left|\det\begin{pmatrix}1 & 0 \\ 0 & 1\end{pmatrix}\right|=1, \quad (20)$$

making use of the fact that the determinant of a product of matrices is equal to the product of the determinants and Eq. (18).

For any function $g(m_1,m_2)$ of the lattice, the discrete space Fourier transform is defined[12,13] as

$$\hat{g}(\mathbf{f})=|A|\sum_{m_1,m_2}g(m_1,m_2)e^{-2\pi i\mathbf{r}_{m_1,m_2}\cdot\mathbf{f}} \quad (21)$$

for all spatial frequencies $\mathbf{f}$. This definition is equivalent to evaluating the z-transform on the unit circle in the complex plane.[12,15] It is also equivalent to the Fourier transform of the function obtained from the data set by interpolation with

sinc functions (e.g., Ref. 16, p. 230). Direct calculation from Eq. (21) gives

$$\hat{g}(\mathbf{f})=\hat{g}(\mathbf{f}+m_1\mathbf{w}_1+m_2\mathbf{w}_2), \quad (22)$$

which shows that $\hat{g}$ is periodic in Fourier space for displacements in the dual lattice and one need only consider values of $\hat{g}$ on one unit cell of this lattice. Any frequency $\mathbf{f}$ outside of this unit cell is an alias of a frequency $\mathbf{f}'$ inside the cell, with $\mathbf{f}-\mathbf{f}'$ in the reciprocal lattice. Viewed another way, the reciprocal lattice divides points in the frequency plane into equivalence classes of points, two points being equivalent if and only if they are separated by a vector in the reciprocal lattice. Any unit cell will contain exactly one point from each equivalence class (except for boundaries), and knowledge of $\hat{g}$ on the unit cell determines $\hat{g}$ on the entire plane. Alternatively, one can consider $\hat{g}$ as being defined on the topological "quotient space," a torus, just as one can consider a function on the real line with period 2π as defined on the unit circle (Ref. 17, p. 155).

The exponential functions in the discrete Fourier transformation satisfy a simple orthogonality condition

$$\iint_K d^2\mathbf{f}\,e^{-2\pi i\mathbf{f}\cdot\mathbf{r}_{m_1,m_2}}e^{2\pi i\mathbf{f}\cdot\mathbf{r}_{n_1,n_2}}=|K|\delta_{m_1,n_1}\delta_{m_2,n_2}, \quad (23)$$

where K is the region corresponding to the unit cell of the reciprocal lattice in the frequency plane and $|K|$ is the area of this region, thus giving

$$g(m_1,m_2)=\iint_K d^2\mathbf{f}\,\hat{g}(\mathbf{f})e^{2\pi i\mathbf{f}\cdot\mathbf{r}_{m_1,m_2}} \quad (24)$$

as the inverse transform. The complex exponentials form a complete set of orthogonal functions, so that any appropriate periodic function of frequency $\mathbf{f}$ can be represented in terms of them. The completeness can also be expressed in terms of a comb function as

$$\sum_{m_1,m_2}e^{2\pi i(\mathbf{f}-\mathbf{f}')\cdot\mathbf{r}_{m_1,m_2}}=|K|\sum_{k_1,k_2}\delta(\mathbf{f}-\mathbf{f}'-\mathbf{f}_{k_1,k_2}), \quad (25)$$

where the equality is interpreted in terms of distributions and the sum on the right-hand side is over the frequencies in the reciprocal lattice.[8,16,17]

For actual finite data sets, one applies the finite Fourier transformation. The discrete space Fourier transformation can be interpreted as a limit of the finite Fourier transformation as the number of equally spaced points in the data set is increased. Specifically, consider a bounded subset of the $\{\mathbf{r}_{n_1,n_2}\}$ such as $\mathscr{R}$ of the form

$$\mathscr{R}=\{\mathbf{r}_{n_1,n_2}|N_1\leq n_1<N_1',N_2\leq n_2<N_2'\}, \quad (26)$$

for which the finite Fourier transform and its inverse are given by

$$\hat{g}(l_1,l_2)=\sum_{\mathbf{r}_{n_1,n_2}\in\mathscr{R}}g(n_1,n_2)e^{-2\pi i\mathbf{f}_{l_1,l_2}\cdot\mathbf{r}_{n_1,n_2}}, \quad (27)$$

$$g(n_1,n_2)=\frac{1}{\Delta N_1\Delta N_2}\sum_{\mathbf{f}_{l_1,l_2}\in\mathscr{H}}\hat{g}(l_1,l_2)e^{2\pi i\mathbf{f}_{l_1,l_2}\cdot\mathbf{r}_{n_1,n_2}}, \quad (28)$$

where $\Delta N_i=N_i'-N_i$. The points in the Fourier space are given by

$$\mathbf{f}_{l_1,l_2} = \frac{l_1}{\Delta N_1}\mathbf{w}_1 + \frac{l_2}{\Delta N_2}\mathbf{w}_2 \tag{29}$$

and

$$\mathscr{K} = \{\mathbf{f}_{l_1,l_2} | L_1 \le l_1 < L_1', L_2 \le l_2 < L_2'\}, \tag{30}$$

where the L's are chosen so that $L_i' - L_i = N_i' - N_i$. The reciprocal relationship [Eq. (18)] between the basis vectors $\{\mathbf{v}_i\}$ and the dual basis vectors $\{\mathbf{w}_i\}$ gives

$$\mathbf{f}_{l_1,l_2} \cdot \mathbf{r}_{n_1,n_2} = \left(\frac{l_1}{\Delta N_1}\mathbf{w}_1 + \frac{l_2}{\Delta N_2}\mathbf{w}_2 \right) \cdot (n_1\mathbf{v}_1 + n_2\mathbf{v}_2)$$

$$= \frac{l_1 n_1}{\Delta N_1} + \frac{l_2 n_2}{\Delta N_2}, \tag{31}$$

which, along with choosing $N_i' = -N_i = N_o/2$ and $L_i = -L_i' = N_o/2$ for N_o even, produces a more conventional representation of the finite Fourier transform.

As the number of data points $\Delta N_1 \Delta N_2$ increases, the spacing between the frequencies $\mathbf{f}_{l_1,l_2}$ decreases, so that in the limit the data points on the lattice extend across the entire plane and the frequency values fill a unit cell of the reciprocal lattice. The finite sum in the FFT [Eq. (27)] approximates (with a factor of $|A|$) the infinite sum in the DFT [Eq. (21)], and for the inverse transform the sum in Eq. (28) (with the introduction of a factor of $|A||K| = 1$) becomes

$$g_{\text{FFT}}(n_1, n_2) = \sum_{\mathbf{f}_{l_1,l_2} \in \mathscr{K}} \frac{|K|}{\Delta N_1 \Delta N_2}(|A|\hat{g}_{\text{FFT}}(l_1, l_2))$$

$$\times e^{2\pi i \mathbf{f}_{l_1,l_2} \cdot \mathbf{r}_{n_1,n_2}}, \tag{32}$$

which approximates the integral used in the inversion of the discrete space Fourier transform, Eq. (24). To illustrate this concept, Fig. 1(e) shows a small rectangular lattice (corresponding to $N_i = -1$, $N_i' = 2$). The circles in Fig. 1(f) represent the corresponding frequency vectors for use with the finite Fourier transform. The box shows the region which would correspond to a unit cell of the reciprocal lattice if the lattice in Fig. 1(e) were extended to an infinite lattice. If the finite lattice shown in Fig. 1(e) were extended (but still finite), the corresponding frequency vectors of the finite Fourier transform would fill the unit cell more and more densely.

It should be noted that if ΔN_1 or ΔN_2 are even, then some of the frequencies at which the finite Fourier transform is defined [shown as the circles in Fig. 1(f)] would lie on the boundary of the unit cell, and such frequencies would have aliases which also lie on the boundary. For example, in the square lattice considered in Fig. 1(f), if one of the frequencies at which the finite Fourier transform is defined fell on the edge of the unit cell, an alias of that frequency would lie on the opposite edge, and a frequency on any corner would be aliased with all of the other corners. In certain sums over frequency components, such as Eq. (28), it is useful to adopt the convention that such sums include exactly one representative from each class of aliased frequencies, so that frequencies falling on the boundary of the unit cell are not counted multiple times. If one uses the "quotient space" point of view, this follows automatically as the aliases correspond to a single point in the quotient space. Alternatively, one might weigh each frequency by a factor (1/2 for frequencies lying on edges and 1/4 for corners) so that each class of aliased frequencies has a total weight of 1 (similar to counting fractional atoms when reckoning the number of atoms in a unit cell of a crystal).

The results pertaining to Fourier transformations and dual lattices which are reviewed in this section have direct generalizations to any number of dimensions, but as the statement of the results for arbitrary finite dimension would be notationally cumbersome, only the two-dimensional results have been explicitly stated. For notational convenience, let $\mathbf{m}$ represent the ordered pair m_1, m_2, so that $g(\mathbf{m}) = g(m_1, m_2)$ and $\mathbf{r_m} = \mathbf{r}_{m_1,m_2}$, and similarly for $\mathbf{k}$, e.g., $\mathbf{f_k} = \mathbf{f}_{k_1,k_2}$.

IV. TRANSFER FUNCTION

The analog of the optical transfer function, which relates the response of the detector to the input signal in frequency space, can now be defined. The input signal $\langle I \rangle$ is a continuous function of the plane. As $\langle I \rangle$ is defined relative to the "flat-field," it is reasonable to assume that $\langle I \rangle$ has compact support, or at least vanishes sufficiently quickly at infinity to leave the quantities considered here well defined. Thus the Fourier transform $\langle \hat{I} \rangle$ is a continuous function of the entire frequency plane. The data $D(\mathbf{r_m})$ are well-defined only at the discrete lattice points $\mathbf{r_m}$, so that the discrete space Fourier transform $\langle \hat{D}(\mathbf{f}) \rangle$ is determined by its values in one unit cell of the reciprocal lattice. Values of $\langle \hat{D} \rangle$ outside of the first unit cell are determined by the periodicity relative to the reciprocal lattice and contain no new information. For spatial frequencies inside the first unit cell, the detector responds at the same frequency as the input signal. For frequencies outside of the first unit cell, the detector responds at an aliased frequency, so it is impossible to uniquely determine the input signal without additional information, although it will be argued in later sections that for reasonable tasks this is not a significant problem.

Each point on the detector grid is assumed to respond linearly to the incident signal, so that the analog of Eq. (1) is

$$\langle D(\mathbf{r_m}) \rangle = \Gamma \int \int d^2\mathbf{r}' P(\mathbf{r_m}, \mathbf{r}')\langle I(\mathbf{r}') \rangle, \tag{33}$$

where P, the analog of the point spread function, represents the response of the detector at $\mathbf{r_m}$ to x-ray light incident at $\mathbf{r}'$, and Γ is a constant for converting x-ray intensity into digital values, generally chosen so that the integral of P with respect to $\mathbf{r}'$ is unity. With a discrete detector, one no longer has full translational invariance, but there remains an invariance under translations which take lattice points to lattice points, assuming that each pixel is identical except for position. Thus we can write

$$P(\mathbf{r_m}, \mathbf{r}') = P(\mathbf{r_m} - \mathbf{r}'), \tag{34}$$

to indicate that the response of a detector element to an input signal depends upon the displacement of the detector ele-

ment from the region to which the signal is applied, but not upon the absolute position of the detector element or the signal, from which it follows[18,19] that

$$\langle D(\mathbf{r}_m)\rangle = \Gamma \int \int d^2\mathbf{r}' P(\mathbf{r}_m - \mathbf{r}')\langle I(\mathbf{r}')\rangle \qquad (35)$$

for each position $\mathbf{r}_m$ of the sensitive elements on the lattice. While the data $D(\mathbf{r}_m)$ are only available at the lattice points, the convolution can be calculated at any point, so that

$$\mathscr{D}(\mathbf{r}) = \Gamma \int \int d^2\mathbf{r}' P(\mathbf{r} - \mathbf{r}')\langle I(\mathbf{r}')\rangle, \qquad (36)$$

$$\hat{\mathscr{D}}(\mathbf{f}) = \Gamma \hat{P}(\mathbf{f})\langle \hat{I}(\mathbf{f})\rangle, \qquad (37)$$

serves as a definition of $\mathscr{D}(\mathbf{r})$ for any position $\mathbf{r}$. Although $\mathscr{D}(\mathbf{r})$ is equal to the data $\langle D(\mathbf{r}_m)\rangle$ at the lattice points where $\mathbf{r} = \mathbf{r}_m$, at other points $\mathscr{D}(\mathbf{r})$ is an interpolation which will not in general represent a physical quantity, although it is sometimes useful to think of $\mathscr{D}(\mathbf{r})$ as the response of a virtual sensitive element added to the detector at position $\mathbf{r}$ in such a manner as to not perturb or be perturbed by the other elements. The discrete space Fourier transform on $\langle D(\mathbf{r}_m)\rangle$ can now be calculated using $\langle D(\mathbf{r}_m)\rangle = \mathscr{D}(\mathbf{r}_m)$ for $g(\mathbf{r}_m)$ in Eq. (21), giving

$$\langle \hat{D}(\mathbf{f})\rangle = |A| \sum_m e^{-2\pi i \mathbf{r}_m \cdot \mathbf{f}} \mathscr{D}(\mathbf{r}_m)$$

$$= |A| \sum_m \int \int_K d^2\mathbf{f}' \, \hat{\mathscr{D}}(\mathbf{f}') e^{2\pi i \mathbf{r}_m \cdot (\mathbf{f}' - \mathbf{f})}$$

$$= \sum_{\mathbf{f_k}} \hat{\mathscr{D}}(\mathbf{f} + \mathbf{f_k}) = \Gamma \sum_{\mathbf{f_k}} T(\mathbf{f} + \mathbf{f_k})\langle \hat{I}(\mathbf{f} + \mathbf{f_k})\rangle, \qquad (38)$$

which follows from expressing $\mathscr{D}$ in terms of its Fourier transform and using the completeness relationship expressed in Eq. (25).

Comparison of Eq. (38) with its screen-film analog, Eq. (2), helps to clarify the interpretation of the OTF, $T(\mathbf{f})$. The spacings in the discrete lattice introduce new length scales which occur explicitly in the summation over aliases. In the limit of a very finely grained lattice, so that $|A| \to 0$, the spacing of the reciprocal lattice points gets larger, until only the one unaliased term contributes significantly to Eq. (38), and the screen-film case is recovered.

When frequencies higher than those supported by the lattice are present in the signal, the summation in Eq. (38) introduces "aliasing," that is, there exist multiple spatial input frequencies whose output is at the same frequency and are thus not distinguishable. For example, considering a one-dimensional lattice with pixel-pitch of 1 cm, oscillations at a rate of 0.5 cycles per cm can not be distinguished from oscillations at a rate of 1.5 cycles per cm. From Eq. (38), two components of the input signal generate the same component of the output signal if and only if their spatial frequencies differ by an element $\mathbf{f}_{k_1,k_2}$ of the reciprocal lattice.

More generally for any lattice there are frequencies $\mathbf{f}_o$ such that $-\mathbf{f}_o$ is an alias of $\mathbf{f}_o$ (for example, if $\mathbf{f}$ and $-\mathbf{f}$ are on opposite boundaries of the first unit cell in the reciprocal

lattice). For such a frequency $\mathbf{f}_o$ [noting that $T(\mathbf{f}) = T^*(-\mathbf{f})$ and $\langle \hat{I}(\mathbf{f})\rangle = \langle \hat{I}^*(-\mathbf{f})\rangle$ for real-valued $P(\mathbf{r})$ and $\langle I(\mathbf{r})\rangle$] it is possible to choose the phase of $\langle \hat{I}(\mathbf{f}_o)\rangle$ so that

$$T(\mathbf{f}_o)\langle \hat{\mathbf{I}}(\mathbf{f}_o)\rangle + \mathbf{T}(-\mathbf{f}_o)\langle \hat{\mathbf{I}}(-\mathbf{f}_o)\rangle = 0, \qquad (39)$$

showing by Eq. (38) that a sinusoidal signal concentrated at frequency $\mathbf{f}_o$ and displaced by an appropriate offset relative to the lattice (as determined by the phase of $\langle I(\mathbf{f}_o)\rangle$) would be indistinguishable from the flat-field signal. Returning to the simple one-dimensional model of pixels spaced at 1 cm, this result means that for some displacement relative to the lattice the input of a sinusoidal wave of frequency 1 cycle/cm would give vanishing output. If the detector elements were assumed to integrate over 1 cm intervals, then the output vanishes for all relative phases of the sinusoidal input wave and the lattice. If, alternatively, the detectors integrated over only 0.5 cm regions but still were spaced at 1.0 cm intervals, then the sinusoidal wave would have vanishing output only when the nodes of the sinusoid fell upon the centers of the 0.5 cm sensitive regions of the detectors and would otherwise change each digital value by a phase-dependent offset from the flat-field value.

The optical transfer function has been written in terms of a Fourier transform using complex exponentials. Since complex-valued exponential inputs are not readily available, it is necessary to ask how T can be experimentally measured. In principle, phantoms machined to produce sinusoidal patterns of x-ray intensity could be used, and by repeated measurements with different offsets one could separate the positive and negative frequency components. A more practical method is the well-known slanted edge technique,[20,21] in which images are acquired under flat-field conditions except that one half-plane of the detector is shielded so as not to receive any input signal. The detector response D as a function of distance from the edge is referred to as the edge-spread function ESF, which can be differentiated[22] to give the line spread function, LSF. Alternatively, by providing an appropriate input the LSF can be acquired directly.[23] The LSF represents integrals through the PSF along lines parallel to the edge, so that by acquiring data with the edge at multiple angles one obtains the radon transform of the PSF. One can reconstruct the PSF, but it is more common to stop after computing the Fourier transform of the ESF, which gives values of the OTF for spatial frequencies $\mathbf{f}$ which are normal to the edge. For discrete-array detectors it is desirable that the slope of the edge is not commensurate with the lattice spacing (for example, on a square grid, if the edge is not parallel to one of the axes and does not have a slope which is a ratio of small whole numbers like 1/2 or 2/3). When this condition is satisfied, for a given region of interest the distances z of the lattice points $\mathbf{r}_m$ from the edge will be distributed sufficiently densely and evenly so that the ESF is said to be "super-sampled," i.e., sampled at a rate significantly higher than the reciprocal of the lattice spacing, so that it is possible to measure values of the OTF for input frequencies beyond those supported by the lattice.

For discrete-array detectors, rotational symmetry will generally be only approximately valid at low spatial frequen-

cies, so it is desirable to make measurements at multiple angles relative to the lattice. When the ESF_θ at a given angle θ is acquired, it is often the case that the precise position of the edge relative to the lattice is not known, so that one actually acquires data for $\mathrm{ESF}_\theta(z + z_\theta)$, where z_θ represents the lack of knowledge of the exact position of the edge. Upon taking the Fourier transform of the ESF, this introduces a phase uncertainty of the form $e^{2\pi i |\mathbf{f}| z_\theta}$ into the value of $T(\mathbf{f})$. While this phase uncertainty also occurs in measurements of screen-film systems, for discrete-array systems summations over aliased frequencies generally are not possible given uncertainties in the relative phases of values of T at different spatial frequencies. In general one can remove this phase uncertainty by redefining the lattice positions to correspond to the ''centers-of-mass'' of the response functions of the sensitive elements. More specifically, if

$$\int \int d^2\mathbf{r} P(\mathbf{r}) = \int dz\, \mathrm{ESF}_\theta(z + z_\theta) > 0, \tag{40}$$

then it is possible to redefine the lattice (by a shift) so that each lattice point sits at the center of mass of the response function of the associated detector element, giving

$$\int \int dx dy\ x P(\mathbf{r}) = \int \int dx dy\ y P(\mathbf{r}) = 0. \tag{41}$$

With this redefinition of the lattice position, each LSF acquired corresponds to a radon projection of the PSF (onto a line perpendicular to the edge) and thus the center of mass of each LSF should be at the origin. This corresponds to shifting the acquired LSF (adjusting z_θ) so that

$$\int dz\, \mathrm{ESF}_\theta(z) z = 0 \tag{42}$$

for each angle.

As a practical matter this results in an increase in the amount of data it is desirable to report for a given detector. If one can assume an inversion symmetry, i.e., $P(\mathbf{r}) = \mathbf{P}(-\mathbf{r})$, then the imaginary part of the transfer function will vanish identically, so that only the real part need be reported. The absolute value of the OTF, traditionally called the modulation transfer function (MTF), gives enough information to calculate quantities such as the spatial average of SNR^2 (Sec. VI), but does not give enough information to explore other aspects of the detector, such as the spatial variation of SNR^2 as the test object is moved relative to the lattice. Researchers should also note that with the slanted edge technique, when combining raster lines to plot the edge spread function, the independent variable of interest is the distance from the edge, which for square lattices differs from the distance along a raster line by a factor of the cosine of the angle between the raster line and the normal to the edge. This factor becomes significant when trying to measure the transfer function at angles away from the detector axes. Based upon the experience of the authors, one can generally measure values of the OTF at frequencies several times the highest frequency supported by the lattice. One is, of course, measuring the response of the detector at low frequency aliases to higher frequency input signals. Whether the pres-

ence of these aliased signals in the output is desirable will depend upon the task at hand. For example, it might be desirable to detect a high-frequency signal even if one can't distinguish it from a low-frequency signal, or the resulting ambiguity might be unacceptable.

The question of what, if anything, should be identified as either the OTF or MTF for digital systems has been addressed in several ways in the literature. For example, Dobbins[24] discusses the ''pre-sampled OTF'' (OTF_{pre}, our T) as measured via the LSF,[23] but then emphasizes the fact that the response to an input signal with either sinusoidal or delta-function spatial variation will change if the input signal is shifted by a fraction of the lattice spacing. This dependence, which follows from Eq. (38) when the input is expanded into Fourier components, confounds attempts to define the MTF either in terms of the frequency response to a single delta function or as the ratio of output-to-input amplitude for a sinusoid. Dobbins addresses this issue by defining

$$\mathrm{OTF}_d(\mathbf{f}) = \sum_{\mathbf{f_l}} \mathrm{OTF}_{pre}(\mathbf{f} + \mathbf{f_l}), \tag{43}$$

and defining $\mathrm{EMTF}(\mathbf{f})$ as the amplitude of the detector response at frequency $\mathbf{f}$ to a delta-function input averaged over all positions of the delta function. Giger and Doi[25] included such a summation of OTF over aliased frequencies in their study of data acquisition and display for digital systems. Both OTF_d and EMTF can be computed in terms of the OTF, but it can be seen that neither is sufficient for calculating SNR. Metz[26] approaches the problem in essentially the same manner as discussed in this paper, and indeed Eqs. (19) and (30) of that paper essentially give our Eq. (38), but for a slightly more specialized case. Metz then brings up the point that a shift by a fraction of the lattice spacing in the input signal does not result in a simple shift in the output data, and concludes that ''the effect is accounted for mathematically, but it prevents us from defining a unique 'transfer function' of the sampling process.''

Experimentally, Sones and Barnes[27] recognized the desirability of measuring the transfer function above the maximum frequency supported by the sampling lattice in their work with a digital radiography unit. This measurement was performed using a novel technique based upon a phantom consisting of periodically arranged wires, the distance between the wires chosen to be incommensurate with the distance between samples acquired by the detector. Fujita, Doi, and Giger[28] measured the ''pre-sampling analog MTF'' above the maximum frequency supported by their sampling lattice via a slanted slit technique and recognized that ''knowledge of the pre-sampling analog MTF ... will be useful in the determination of signal-to-noise ratio (SNR) [and] the evaluation of digital systems,'' a statement with which we heartily agree.

Working from a complementary theoretical perspective, Barrett et al.[1] uses the ''cross-talk'' matrix to address the more general case of any detector whose response is linear, then proceeds to more specialized cases. In Barrett et al., the input to the system is defined as the object being imaged

parameterized in terms of the coefficients of its three-dimensional Fourier series, while for our purposes the input is the x-ray fluence incident on the detector. For projection radiography, which is our primary interest, the incident x-ray fluence is directly related to the integrated attenuation coefficient of the object along rays diverging from the x-ray focus, at least to a first approximation. As our goal is to attempt to quantify the detector response independently of other technical factors, this approximation is adequate. Barrett *et al.* is concerned with detectors which may have relatively few sensitive elements, so the application of Fourier techniques to the acquired data is not considered. Barrett *et al.* applies the cross-talk matrix to the case of a one-dimensional array of detector elements with aperture size equal to the element spacing, and finds that the cross-talk between components of the input at separate frequencies decreases as the length of the array is increased, so long as the frequencies are not aliases of each other. Thus in the limit of a homogeneous detector of infinite extent one recovers the fact that the transfer function behaves as a sparse matrix, in which all terms vanish except those on the diagonal or relating aliased frequencies.

In order to use Eq. (38) to calculate the response of the detector to a given input, it would be necessary to know the position of the object being imaged with a precision finer than the lattice spacing. Strictly speaking, to calculate the response in either the discrete or continuous case requires that the input be ''perfectly known.'' However, in the case of a continuous detector, a shift in position of the input will result in a corresponding shift in position of the output, while for a discrete detector the ''shape'' of the output would change. In many cases, such as predicting the detectability of randomly placed objects, one would need to calculate for an ensemble of objects displaced with random phases relative to the lattice, as will be illustrated below in calculating the SNR of small objects.

V. NOISE

Individual realizations of an imaging process have an irreducible variability which sets a fundamental limit on how effectively the detector can distinguish between various inputs. For discrete-array systems, as for screen-film systems, the noise can be quantified in terms of the autocovariance function. If the noise is additive and Gaussian, then the autocovariance matrix completely summarizes the stochastic process which generates the noise. If the system is also stationary, then Fourier techniques can be used to define the Wiener spectrum.

The discrete autocovariance function is given by[13,15]

$$C(\mathbf{r_m}, \mathbf{r_n}) = \langle D(\mathbf{r_m}) D(\mathbf{r_n}) \rangle, \tag{44}$$

where $\mathbf{r_m}$ and $\mathbf{r_n}$ are points in the lattice of detectors, the angled brackets represent averaging over an ensemble of flatfield images, and as discussed above $\langle D(\mathbf{r_m}) \rangle = 0$ in the absence of a signal. Symmetry under interchange of positions

$$C(\mathbf{r_m}, \mathbf{r_n}) = C(\mathbf{r_n}, \mathbf{r_m}) \tag{45}$$

is an immediate result. With the assumption of stationarity, the autocovariance depends only upon the displacement $\mathbf{r_m} - \mathbf{r_n}$, so we can write

$$C(\mathbf{r_m}, \mathbf{r_n}) = C(\mathbf{r_m} - \mathbf{r_n}) \tag{46}$$

without ambiguity. Note that the difference between two vectors corresponding to lattice points is again a vector corresponding to a lattice point, so C on the right-hand side of Eq. (46) is defined at precisely the lattice points.

The Wiener spectrum $W(\mathbf{f})$ is defined as the discrete space Fourier transform [Eq. (21)] of the autocovariance function $C(\mathbf{r_m})$. As with any discrete space Fourier transform, the Wiener spectrum is periodic in frequency space [Eq. (22)] so that one need only consider the values of $W(\mathbf{f})$ on a single unit cell of the reciprocal lattice. It is noteworthy that both the autocovariance C and the Wiener spectrum W are real-valued and even. As with screen-film systems, one considers statistics which are linear functions of the data, so if $g(m_1, m_2)$ is a set of real (or complex) numbers defined on the lattice points, one defines

$$\theta_g = |A| \sum_{\mathbf{r_m}} g(\mathbf{m}) D(\mathbf{r_m}). \tag{47}$$

The variance of θ_g (for g complex valued, the sum of the variances of the real and complex parts) is given by

$$\mathrm{Var}(\theta_g) = \langle \theta_g \theta_g^* \rangle \tag{48}$$

$$= |A|^2 \left\langle \left(\sum_{\mathbf{m}} g(\mathbf{m}) D(\mathbf{r_m}) \right) \left(\sum_{\mathbf{n}} g^*(\mathbf{n}) D(\mathbf{r_n}) \right) \right\rangle \tag{49}$$

$$= |A|^2 \sum_{\mathbf{m}} \sum_{\mathbf{n}} g(\mathbf{m}) C(\mathbf{r_n} - \mathbf{r_m}) g^*(\mathbf{n}) \tag{50}$$

in terms of real space. Expressing the autocovariance matrix as the inverse discrete space Fourier transform [Eq. (24)] of the Wiener spectrum one obtains

$$\mathrm{Var}(\theta_g) = |A|^2 \sum_{\mathbf{m}} \sum_{\mathbf{n}} g(\mathbf{m}) \int \int_K d^2 \mathbf{f}$$
$$\times W(\mathbf{f}) e^{2\pi i \mathbf{f} \cdot (\mathbf{r_n} - \mathbf{r_m})} g^*(\mathbf{n}) \tag{51}$$

$$= \int \int_K d^2 \mathbf{f} \hat{g}(\mathbf{f}) \hat{g}^*(\mathbf{f}) W(\mathbf{f}), \tag{52}$$

where the second step follows from the definition of the discrete space Fourier transform [Eq. (21)].

Thus one can calculate the variance of a statistic θ_g, which depends in a linear manner upon the data, using either the autocovariance function or the Wiener spectrum. Statistics of this form, for $g(\mathbf{m})$ real-valued, will be seen to correspond to decision variables of ideal observers in Sec. VI. As in the screen-film case, it is useful to consider functions $g(\mathbf{m})$ corresponding to the product of a plane wave and a windowing function, which can be written as

$$g_{\mathbf{f}_o}(\mathbf{m}) = G(\mathbf{m}) e^{2\pi i \mathbf{f}_o \cdot \mathbf{r_m}}, \tag{53}$$

where $G(\mathbf{m})$ is a real-valued window function with normalization

$$|A| \sum_{\mathbf{m}} G(\mathbf{m}) G^*(\mathbf{m}) = 1, \quad \int \int_K d^2 \mathbf{f} \hat{G}(\mathbf{f}) \hat{G}^*(\mathbf{f}) = 1, \quad (54)$$

where the two normalizations are equivalent by Parseval's theorem. Applying Eq. (49) and Eq. (52),

$$\mathrm{Var}(\theta_g) = |A|^2 \left\langle \left| \sum_{\mathbf{m}} G(\mathbf{m}) e^{-2\pi i \mathbf{f}_o \cdot \mathbf{r_m}} D(\mathbf{r_m}) \right|^2 \right\rangle \quad (55)$$

$$= \int \int_K d^2 \mathbf{f} |\hat{G}(\mathbf{f} - \mathbf{f}_o)|^2 W(\mathbf{f}). \quad (56)$$

For suitable windowing functions G, $|\hat{G}(\mathbf{f} - \mathbf{f}_o)|^2$ will be strongly peaked near $\mathbf{f}_o$ so that one obtains an estimate of the Wiener spectrum at the specified frequency, $W(\mathbf{f}_o)$. In particular, if $G_{\mathrm{rect}}(\mathbf{m})$ is chosen as $1/(M_1 M_2 |A|)^{1/2}$ at the lattice points $\mathbf{m} \in [0,...,M_1 - 1] \times [0,...,M_2 - 1]$, then

$$\theta_{\mathrm{rect}} = \sum_{m_1=0}^{M_1-1} \sum_{m_2=0}^{M_2-1} \frac{1}{\sqrt{M_1 M_2 |A|}} D(\mathbf{r_m}) e^{2\pi i \mathbf{f}_o \cdot \mathbf{r_m}}, \quad (57)$$

$$|\hat{G}(\mathbf{f} - \mathbf{f}_o)|^2 = \frac{|A|}{M_1 M_2} \frac{\sin^2(M_1 \pi (\mathbf{f} - \mathbf{f}_o) \cdot \mathbf{v}_1)}{\sin^2(\pi (\mathbf{f} - \mathbf{f}_o) \cdot \mathbf{v}_1)}$$

$$\times \frac{\sin^2(M_2 \pi (\mathbf{f} - \mathbf{f}_o) \cdot \mathbf{v}_2)}{\sin^2(\pi (\mathbf{f} - \mathbf{f}_o) \cdot \mathbf{v}_2)}, \quad (58)$$

which explicitly shows that for this choice of G, $|\hat{G}(\mathbf{f} - \mathbf{f}_o)|^2$ is strongly peaked near $\mathbf{f}_o$. For a square lattice with conventional choice of basis vectors, $(\mathbf{f} - \mathbf{f}_o) \cdot \mathbf{v}_1 = (f_x - (f_o)_x) \Delta x$, where $f_x - (f_o)_x$ is the difference in the x components of the frequencies and Δx is the lattice spacing in the x direction, and similarly for the y axis. In general, if a separable window is chosen, so that $G(\mathbf{m}) = G_1(m_1) G_2(m_2)$, then $\hat{G}(\mathbf{f}) = \hat{G}_1(\mathbf{f} \cdot \mathbf{v}_1) \hat{G}_2(\mathbf{f} \cdot \mathbf{v}_2)$, so that one can make use of the variety of one-dimensional windows which have been studied.[29]

Returning to the case of a general lattice, Eq. (58) shows that for this particular choice of window, as is typical, the estimate of $W(\mathbf{f})$ becomes sharper as the spatial width of the window increases, so that

$$W(\mathbf{f}) = \hat{C}(\mathbf{f}) = \lim_{M_1, M_2 \to \infty} \langle W_{M_1 M_2}(\mathbf{f}) \rangle, \quad (59)$$

$$W_{M_1 M_2}(\mathbf{f}) = \frac{|A|}{M_1 M_2} \left| \sum_{m_1=0}^{M_1-1} \sum_{m_2=0}^{M_2-1} D(\mathbf{r_m}) e^{-2\pi i \mathbf{f} \cdot \mathbf{r_m}} \right|^2, \quad (60)$$

where, by stationarity, any $M_1 \times M_2$ region of the detector lattice will serve. Specializing to the zero frequency case, $\mathbf{f} = \mathbf{0}$, one gets

$$W(\mathbf{0}) = \lim_{M_1, M_2 \to \infty} (M_1 M_2 |A|)$$

$$\times \left\langle \left(\frac{1}{M_1 M_2} \sum_{m_1=0}^{M_1-1} \sum_{m_2=0}^{M_2-1} D(\mathbf{r_m}) \right)^2 \right\rangle, \quad (61)$$

which is the discrete-array version of Selwyn granularity[5] (the variance in the average digital value corresponds to the variance in the spatially averaged optical density of film). Comparing Eq. (61) to Eq. (52), one can interpret Eq. (61) as the statement that the integrated response over large regions of the detector depends only upon the low-frequency components of the Wiener spectrum. Viewed spatially, this result means that the digital values averaged over sufficiently large disjoint regions are approximately independent, so that the variance of the average over N large subregions scales with $1/N \propto 1/M_1 M_2$.

As with the OTF, the results of the screen-film theory appear as a limiting case for sufficiently fine lattices. Writing Eqs. (59) and (60) as

$$W(\mathbf{f}) = \lim_{M_i \to \infty} \frac{1}{M_1 M_2 |A|}$$

$$\times \left\langle \left| \sum_{m_1=0}^{M_1-1} \sum_{m_2=0}^{M_2-1} |A| D(\mathbf{r_m}) e^{-2\pi i \mathbf{f} \cdot \mathbf{r_m}} \right|^2 \right\rangle, \quad (62)$$

the summations become approximations of the integrals in Eq. (6).

The discrete autocovariance [Eq. (44)], the definition of the Wiener spectrum as the discrete space Fourier transform of the autocovariance, and the use of Fourier components of flat-field images to estimate the NPS [Eq. (59)] have occurred in several places in the medical physics literature,[13,30] but historically these results seem to have been considered less than satisfactory from a theoretical point of view. For example, Cunningham[31] stated that while ''[i]t is tempting to write out the NPS of [the sampled digital signal], but strictly speaking this violates the shift-invariance assumption since [the data] is sampled and is therefore not shift invariant.'' More recently, Cunningham,[32] in analyzing the concept of NPS in terms of cyclostationary[15,33] random processes, defines $W_{M_1 M_2}$ [Eq. (60)] as ''a working definition of the digital NPS.'' As detailed in Sec. VI, the NPS, as defined here, is precisely the noise which sets the detection-theoretic limits on the use of the detector. In the detection-theoretic approach of Barrett et al.,[1] the Fisher information matrix relates the detector noise back into uncertainties in the estimates of the Fourier coefficients of the object being imaged. This has the advantage that it removes the fundamentally arbitrary choice of scale in using digital values, but if aliased frequencies become important the Fisher information matrix becomes singular so that the inversion of this matrix is problematic.

The definition of NPS given here is intended to be operational in the sense that it is defined in a manner which can be implemented using the experimentally available digital values. For the purposes of understanding the sources of noise in detectors, it may be useful to consider the noise in the ''presampled'' signal, and for some detectors this presampled signal might be experimentally accessible. For example, in a detector based on a phosphor screen coupled with a lens to a charge-coupled device (CCD) camera, one could do experiments in which the camera is replaced by a photographic film. For some devices, such as TFT arrays using direct conversion mechanisms, the meaning of the presa-

mpled signal is less clear as removal or refinement of the sampling array is likely to change the electric fields responsible for charge collection.

As reviewed by Wagner and Sandrik,[30] the calculation of the NPS can be implemented in several ways. One method is to estimate the autocovariance function [Eqs. (44) and (46)] using pairs of points in one or (preferably) more images, and then performing the Fourier transform to give the NPS. Alternatively, the variance in the Fourier components is used, as in Eq. (55). If G is chosen as a rectangular window, then Eq. (55) reduces to Eq. (59), so that $\langle W_{M_1 M_2}(\mathbf{f}) \rangle$ [Eq. (60)] is used as an estimate of $W(\mathbf{f})$. In principle the frequency $\mathbf{f}$ is a continuous variable, but the spread of $|\hat{G}(\mathbf{f})|^2$ limits the resolution in frequency space [by Eq. (56)] and this spread is inversely proportional to the size of the spatial region and on the order of $|K|/M_1 M_2$. Given this resolution, it is reasonable to calculate the NPS at $M_1 M_2$ frequencies spaced evenly in the unit cell K in frequency space. Thus, the techniques commonly in use by experimenters give precisely the quantities of interest from our current theoretical point of view, although the use of windows other than the rectangular window might be of interest to obtain better frequency resolution.

Generally, frequency resolution is not a limiting factor in estimating the Wiener spectrum, and the NPS estimated by $\langle W_{M_1 M_2}(\mathbf{f}) \rangle$ is subjected to further smoothing. From Eq. (57) it is seen that $\langle W_{M_1 M_2}(\mathbf{f}_o) \rangle$ is the variance in the random variable θ_{rect}, and as the region of interest used in the calculation is made larger, the variance in θ_{rect} tends to $W(\mathbf{f})$ which will be nonzero in general. Because the variance of θ_{rect} does not vanish, neither will the variance in $|\theta_{\text{rect}}|^2$, so the variance in $W_{M_1 M_2}(\mathbf{f})$ does not converge to zero as $M_1, M_2 \to \infty$. As the region of interest is made larger, one gains in spectral resolution but not precision, and this represents an unavoidable trade-off.[30,34] One can only decrease the uncertainty in the estimates of the Wiener spectra by averaging estimates of $W(\mathbf{f})$ from several different regions of interest. Of course, for the purposes of analysis one could divide a large region into several smaller regions, and the averaged value of estimates of $W(\mathbf{f})$ would then have less uncertainty, but the spectral blur would be increased. Since it is often inconvenient to obtain sufficiently many flat-field images to make the standard error in the estimates of $W(\mathbf{f})$ at individual frequencies small, researchers often opt for smoothing the experimental spectrum.

VI. KNOWN SIGNAL DETECTION

Having addressed the issues of OTF and Wiener spectrum, it is now possible to use the signal-to-noise ratio (SNR) to quantify the ability of the detector to perform SKE/BKE tasks. First, however, it is useful to briefly review the meaning of the SNR in terms of an ideal[9,35] observer working with Gaussian statistics. The ideal observer is challenged with deciding between two hypotheses based upon a given set of data. In the current context, these data consist of the digital values obtained from the detector, and for the moment we will restrict the observer to knowledge of only a finite region of the detector, corresponding to indexes $\mathbf{m} \in \mathcal{M} = [M_1, \ldots, M_1' - 1] \times [M_2, \ldots, M_2' - 1]$. This observer works under the assumption that given hypothesis H_I, corresponding to an expected input signal $\langle I(\mathbf{r}) \rangle_\mathrm{I}$ and an expected data set $\langle D(\mathbf{r_m}) \rangle_\mathrm{I}$, the probability density function describing the expected range and frequency of observed data sets is Gaussian. This Gaussian distribution in $(M_1' - M_1) \times (M_2' - M_2) = \Delta M_1 \Delta M_2$ dimensions, one dimension for each detector element available to the observer, can be written explicitly, but to make the formulas somewhat less cumbersome we use the following notation: $X_\mathbf{m} = D(\mathbf{r_m})$, $\langle X_\mathbf{m} \rangle_\mathrm{I} = \langle D(\mathbf{r_m}) \rangle_\mathrm{I}$, $\langle X_\mathbf{m} \rangle_\mathrm{II} = \langle D(\mathbf{r_m}) \rangle_\mathrm{II}$, and $\{X_\mathbf{m}\} = \{D(\mathbf{r_m}) | \mathbf{m} \in \mathcal{M}\}$ is a $\Delta M_1 \Delta M_2$-dimensional vector in the space of all possible data values for the detector elements in region $\mathcal{M}$. The probability distribution which governs the frequency with which particular data sets will be obtained under hypothesis H_I is given by

$$P_\mathrm{I}(\{X_\mathbf{m}\}) = N_o e^{-1/2 \sum_{\mathbf{m}, \mathbf{n} \in \mathcal{M}} (X_\mathbf{m} - \langle X_\mathbf{m} \rangle_\mathrm{I})(\mathbf{C}^{-1})_{\mathbf{mn}} (X_\mathbf{n} - \langle X_\mathbf{n} \rangle_\mathrm{I})},$$

(63)

where the normalization factor is given by

$$N_o = \left(\frac{1}{2\pi} \right)^{(\Delta M_1 \Delta M_2)/2} \frac{1}{\sqrt{\det \mathbf{C}}}.$$

(64)

The matrix $\mathbf{C_{mn}}$ is the autocovariance function $C(\mathbf{r_m}, \mathbf{r_n})$ of Sec. V restricted to the range $\mathbf{m}, \mathbf{n} \in \mathcal{M}$. The fact that $\mathbf{m}$ and $\mathbf{n}$ are double indices, e.g., $\mathbf{m}$ stands for m_1, m_2, is not a problem from the theoretical point of view, and in principle for a numerical calculation one could simply choose a convenient one-to-one pairing of the double indices $m_1, m_2 \in \mathcal{M}$ with the integers $1, \ldots, \Delta M_1 \Delta M_2$ so that $\mathbf{C}$ would be indexed in a more customary manner. Under hypothesis H_II, the range and frequency of observed data sets will be governed by a Gaussian probability density P_II, this time concentrated around $\langle X \rangle_\mathrm{II}$. The restricted covariance matrix, $\mathbf{C}$, occurring in both cases, will be the same under the assumption that the noise is additive.

Returning to the question of how to decide between hypothesis H_I and hypothesis H_II, if for a given instance of the experiment a data set $\{X_\mathbf{m}\} = \{D(\mathbf{r_m}) | \mathbf{m} \in \mathcal{M}\}$ is obtained such that $P_\mathrm{II}(\{X_\mathbf{m}\})$ is relatively large and $P_\mathrm{I}(\{X_\mathbf{m}\})$ is relatively small, it would generally be reasonable to favor H_II. Thus the ideal observer's decision rule based on the likelihood ratio $P_\mathrm{II}/P_\mathrm{I}$, as discussed below, is intuitively reasonable.

The ideal observer attempts to minimize the expected cost[9,36] given knowledge of the cost of misclassification under either hypothesis and the a priori probabilities associated with each hypothesis,

$$\langle \text{Cost} \rangle = P(H_\mathrm{I}) P(\text{ChII}|\text{I}) C_{\mathrm{I} \to \mathrm{II}} + P(H_\mathrm{II}) P(\text{ChI}|\text{II}) C_{\mathrm{II} \to \mathrm{I}},$$

(65)

where in the first term $P(H_\mathrm{I})$ is the a priori probability of the state corresponding to hypothesis H_I being true, $P(\text{ChII}|\text{I})$ is the probability of mistakenly choosing hypothesis H_II when hypothesis H_I is correct, $C_{\mathrm{I} \to \mathrm{II}}$ is the cost associated with this error, and similarly for the second term. Given a region R_II

of the $\Delta M_1 \Delta M_2$ dimensional data space and the decision rule that, if the observed data $\{D(\mathbf{r_m})|\mathbf{m} \in \mathscr{M}\}$ are in R_{II} then the observer rules in favor of hypothesis H_{II} and otherwise in favor of H_{I}, then the probability of mistakenly favoring hypothesis H_{II} when H_{I} is correct is

$$P(\mathrm{ChII}|\mathrm{I}) = \int \int \cdots \int_{R_{\mathrm{II}}} d^{\Delta M_1 \Delta M_2}\{X_\mathbf{m}\} P_{\mathrm{I}}(\{X_\mathbf{m}\}), \qquad (66)$$

and, as under either hypothesis the total probability must be unity,

$$P(\mathrm{ChI}|\mathrm{II}) = 1 - \int \int \cdots \int_{R_{\mathrm{II}}} d^{\Delta M_1 \Delta M_2}\{X_\mathbf{m}\} P_{\mathrm{II}}(\{X_\mathbf{m}\}) \quad (67)$$

gives the probability of making the error in the other direction. Combining Eqs. (65)–(67),

$$\langle \mathrm{Cost} \rangle = P(H_{\mathrm{II}}) C_{\mathrm{II} \to \mathrm{I}}$$
$$+ \int \int \cdots \int_{R_{\mathrm{II}}} d^{\Delta M_1 \Delta M_2}\{X_\mathbf{m}\} \mathrm{DC}(\{X_\mathbf{m}\}), \qquad (68)$$

where

$$\mathrm{DC}(\{X_\mathbf{m}\}) = P(H_{\mathrm{I}}) C_{\mathrm{I} \to \mathrm{II}} P_{\mathrm{I}}(\{X_\mathbf{m}\})$$
$$- P(H_{\mathrm{II}}) C_{\mathrm{II} \to \mathrm{I}} P_{\mathrm{II}}(\{X_\mathbf{m}\}) \qquad (69)$$

is the differential cost which, if the experiment were repeated sufficiently often, would be attributed to those experiments which gave data $\{D(\mathbf{r_m})|\mathbf{m} \in \mathscr{M}\}$. Clearly the expected cost given by Eq. (68) is minimized by choosing the region R_{II} to be precisely the region where the differential cost DC is negative, so that the ideal observer's decision rule is to choose hypothesis H_{II} if and only if the likelihood ratio

$$\Lambda = \frac{P_{\mathrm{II}}(\{D(\mathbf{r_m})|\mathbf{m} \in \mathscr{M}\})}{P_{\mathrm{I}}(\{D(\mathbf{r_m})|\mathbf{m} \in \mathscr{M}\})} \qquad (70)$$

exceeds the threshold value

$$\Lambda_o = \frac{P(H_{\mathrm{I}}) C_{\mathrm{I} \to \mathrm{II}}}{P(H_{\mathrm{II}}) C_{\mathrm{II} \to \mathrm{I}}}. \qquad (71)$$

By adjusting the operating point Λ_o one makes trade-offs in the rates of the two possible error types, as can be shown graphically in terms of receiver operator curves (ROC analysis).[37] Equivalently one can place the cutoff on $\log \Lambda$, and from Eq. (63),

$$\log \Lambda = \sum_{\mathbf{m},\mathbf{n} \in \mathscr{M}} (\langle D(\mathbf{r_m}) \rangle_{\mathrm{II}} - \langle D(\mathbf{r_m}) \rangle_{\mathrm{I}})(\mathbf{C}^{-1})_{\mathbf{mn}} D(\mathbf{r_n})$$
$$+ \mathrm{const}, \qquad (72)$$

where the constant term does not depend upon the observed data. Thus an ideal observer, viewing a finite region $\mathscr{M}$ of the detector array, uses a linear statistic $\theta_{\mathscr{M}}$ defined by

$$\theta_{\mathscr{M}} = \sum_{\mathbf{m} \in \mathscr{M}} g_{\mathscr{M}}(\mathbf{r_m}) D(\mathbf{r_m}), \qquad (73)$$

where $g_{\mathscr{M}}$ is given implicitly by

$$\sum_{\mathbf{m} \in \mathscr{M}} g_{\mathscr{M}}(\mathbf{r_m}) C(\mathbf{r_m},\mathbf{r_n}) = (\langle D(\mathbf{r_n}) \rangle_{\mathrm{II}} - \langle D(\mathbf{r_n}) \rangle_{\mathrm{I}}), \qquad (74)$$

for all $\mathbf{n} \in \mathscr{M}$. On physical grounds, the values of the mask function $g_{\mathscr{M}}(\mathbf{r_m})$ will be significant only in the region near where $\langle I(\mathbf{r}) \rangle_{\mathrm{II}} - \langle I(\mathbf{r}) \rangle_{\mathrm{I}}$ is nonzero. Further from this region, the values of $g_{\mathscr{M}}(\mathbf{r_m})$ will tend to zero, so that for sufficiently large $\Delta M_1 \Delta M_2$ the ability of the detector to discriminate between the two hypotheses should not depend upon the exact value of $\Delta M_1 \Delta M_2$. In that limit, the efficacy of the detector for the SKE/BKE task should be set by the linear statistic θ_g for the ideal observer's mask function $g_{\mathcal{I}}$. This mask function is defined implicitly by

$$|A| \sum_{\mathbf{m} \in \mathscr{M}} g_{\mathcal{I}}(\mathbf{r_m}) C(\mathbf{r_m},\mathbf{r_n}) = (\langle D(\mathbf{r_n}) \rangle_{\mathrm{II}} - \langle D(\mathbf{r_n}) \rangle_{\mathrm{I}}), \qquad (75)$$

where a factor of $|A|$ is introduced to simplify the form of the solution which in the Fourier domain is given by

$$\hat{g}_{\mathcal{I}}(\mathbf{f}) = \frac{\langle \hat{D}(\mathbf{f}) \rangle_{\mathrm{II}} - \langle \hat{D}(\mathbf{f}) \rangle_{\mathrm{I}}}{W(\mathbf{f})} \qquad (76)$$

$$= \Gamma \frac{\Sigma_{\mathbf{f_k}}(\langle \hat{I}(\mathbf{f}+\mathbf{f_k}) \rangle_{\mathrm{II}} - \langle \hat{I}(\mathbf{f}+\mathbf{f_k}) \rangle_{\mathrm{I}}) T(\mathbf{f}+\mathbf{f_k})}{W(\mathbf{f})}. \qquad (77)$$

The statistic θ_g is itself a Gaussian variable whose variance can be computed using Eq. (52), so that

$$\mathrm{SNR}_{\mathcal{I}}^2 = \Gamma^2 \int_K d^2\mathbf{f} \frac{|\Sigma_{\mathbf{f_k}} \langle \Delta I(\mathbf{f}+\mathbf{f_k}) \rangle T(\mathbf{f}+\mathbf{f_k})|^2}{W(\mathbf{f})} \qquad (78)$$

gives the SNR corresponding to the use of the statistic, as defined in Eq. (8). Thus the limiting case of a detector array of infinite extent is well defined, for pixels ''far away'' from the region of interest do not significantly contribute to the decision. Physically, it is clear that the ''tails'' of the PSF and autocovariance functions set the relevant scale by which distance from the edge of the array is measured, so that when the projected images of objects appear at a distance from the boundary of several times the lengths of these tails the detector can be treated as essentially infinite and Eq. (78) is valid.

It is acknowledged that there are mathematical subtleties related to a truly infinite detector which are not addressed here. For example,[38] the data set for such a detector would represent an infinite set of random variables, so it is not possible to write down a probability density distribution like Eq. (63) in the infinite case. The nature of the physical limit is sufficiently clear that a study of these mathematical subtleties could not change the results. In any case, the fact that the linear statistic θ_g with $g = g_{\mathcal{I}}$ gives the optimal SNR of any linear statistic can be proven directly. More precisely, if $g(\mathbf{r_m})$ is used to define a linear statistic θ_g, then letting $\Delta D = \langle D \rangle_{\mathrm{II}} - \langle D \rangle_{\mathrm{I}}$,

$$\left| \int \int_K d^2\mathbf{f} g(\mathbf{f}) \Delta\hat{D}(\mathbf{f}) \right|^2 = \left| \int \int_K d^2\mathbf{f} (g(\mathbf{f})\sqrt{W(\mathbf{f})}) \right.$$

$$\left. \times \left(\frac{\Delta\hat{D}(\mathbf{f})}{\sqrt{W(\mathbf{f})}} \right) \right|^2$$

$$\leq \int \int_K d^2\mathbf{f} |g(\mathbf{f})|^2 W(\mathbf{f})$$

$$\times \int \int_K d^2\mathbf{f} \frac{|\Delta\hat{D}(\mathbf{f})|^2}{W(\mathbf{f})}, \qquad (79)$$

where the second step is an application of the Schwarz inequality. Dividing both sides of Eq. (79) by the first factor on the right, one obtains

$$\frac{|\int\int_K d^2\mathbf{f} g(\mathbf{f})\Delta\hat{D}(\mathbf{f})|^2}{\int\int_K d^2\mathbf{f}|g(\mathbf{f})|^2 W(\mathbf{f})} \leq \int \int_K d^2\mathbf{f} \frac{|\Delta\hat{D}(\mathbf{f})|^2}{W(\mathbf{f})}, \qquad (80)$$

where the quantity on the left is the SNR^2 for the statistic θ_g [Eqs. (8) and (52)] and the quantity on the right, proven to be larger, is the SNR^2 of the ideal observer as given by Eq. (78) [with Eq. (38)].

As a slightly less subtle point, the construction of the ideal observer involves dividing by $W(\mathbf{f})$, which is problematic if $W(\mathbf{f})=0$ at some frequency. For physical detectors, the Wiener spectrum never vanishes as there is always some residual noise. Even for highly idealized detectors, the Wiener spectrum must reflect the noise in the incident x-ray fluence so that it can only disappear at frequencies where the OTF vanishes, and at these frequencies the Wiener spectrum will vanish no faster than OTF$^2(\mathbf{f})$ (discussed in more detail in the next section), so that even in this case the SNR as given by Eq. (78) is a well-defined limit.

The SNR given by Eq. (78) corresponds to the SKE/BKE decision task using a discrete-array detector, as Eq. (13) gives the SNR for the SKE/BKE decision task for screen-film. Strictly, these formulas do not apply to the task of detection when the observer does not know the position of the object being imaged. For detecting a signal of unknown location, one can calculate the ideal observer's SKE/BKE $\theta_T(\mathbf{r})$ for each possible position $\mathbf{r}$ of the object. A common strategy is then to apply a threshold to $\theta_T(\mathbf{r})$. Under the assumption of Gaussian statistics with complete knowledge except for position, the likelihood ratio computed by the ideal observer uses $\theta_T(\mathbf{r})$ in a nonlinear manner[35,39,40] that is sensitive to peaks in $\theta_T(\mathbf{r})$. In either case, the values of SNR given by Eqs. (13) and (78) are indicative of the efficacy of the ideal observer in the more general case of the position being unknown.

For the discrete-array detector, however, the value of the SNR for the SKE/BKE case will depend upon exactly where the object is relative to the lattice. While this variation can be significant (for example detectors could have interstitial spaces where objects completely disappear), the magnitude of the effect decreases for objects large relative to the lattice spacing. Examples of this for several simple model detectors will be given in the next section. If the variation in SNR^2

with position is not too great, then the spatially averaged value of SNR^2 will be of use.[1] This spatial average can be computed exactly by noting that if an object is shifted by a displacement $\mathbf{r}$, the Fourier transform is multiplied by $e^{2\pi i \mathbf{f}\cdot\mathbf{r}}$ so that in Eq. (78) the sum over elements of the reciprocal lattice becomes

$$\left| \sum_{\mathbf{f}_\mathbf{k}} \langle \Delta\hat{I}(\mathbf{f}+\mathbf{f}_\mathbf{k}) \rangle T(\mathbf{f}+\mathbf{f}_\mathbf{k}) e^{2\pi i \mathbf{f}_\mathbf{k}\cdot\mathbf{r}} \right|^2, \qquad (81)$$

where a common factor independent of $\mathbf{k}(|e^{2\pi i \mathbf{f}\cdot\mathbf{r}}|=1)$ has been removed. In averaging over positions $\mathbf{r}$ in Eq. (78), the denominator of the integrand does not depend upon $\mathbf{r}$, and the numerator is the square of the magnitude of a Fourier series in $\mathbf{r}$, so that in integrating over $\mathbf{r}$ to obtain the average over all displacements one can apply Parseval's theorem to obtain

$$\langle SNR^2 \rangle = \Gamma^2 \int \int_K d^2\mathbf{f} \frac{\Sigma_{\mathbf{f}_\mathbf{k}}|\Delta\hat{I}(\mathbf{f}+\mathbf{f}_\mathbf{k})|^2 |T(\mathbf{f}+\mathbf{f}_\mathbf{k})|^2}{W(f)}$$

$$= \Gamma^2 \int \int d^2\mathbf{f} \left(\frac{|T(\mathbf{f})|^2}{W(\mathbf{f})} \right) |\Delta\hat{I}(\mathbf{f})|^2, \qquad (82)$$

where the second step follows from noting that the sum of the integrals over each unit cell is equivalent to the integral over the entire plane.

As for the OTF and NPS, the film-screen result, Eq. (13), can be recovered from the discrete-array result [Eq. (78)] by going to the limit of a sufficiently fine lattice, in which case the distance to the first aliased frequency is so large that only the unaliased term contributes to Eq. (78). Similarly, for a sufficiently fine lattice all objects are large relative to the lattice spacing, so that SNR^2 does not vary appreciably as the object is moved relative to the lattice spacing. These facts prompt the identification[1] of

$$GNEQ(\mathbf{f}) = \Gamma^2 |T(\mathbf{f})|^2 \Phi^2 / W(\mathbf{f}), \qquad (83)$$

as a generalization of the concept of noise equivalent quantum flux (NEQ), where Φ is the incident x-ray flux, and

$$GDQE(\mathbf{f}) = \Gamma^2 |T(\mathbf{f})|^2 \Phi / W(\mathbf{f}), \qquad (84)$$

as a generalized detective quantum efficiency (DQE). These results parallel the screen-film theory, except that factors of fluence appear in the numerator as the response of digital detectors is linear with fluence [Eq. (33)] while film density is linear with respect to the log of fluence [Eq. (1)]. While Eq. (82) is exact in the context of the assumptions we have made about the detector, SNR^2 enters nonlinearly into other quantities such as the various probabilities of misclassification for a given operating point (sometimes called the false positive fraction and the false negative fraction in ROC methodology). However, when the variation in SNR^2 is not too large, perhaps as measured by the rms (root-mean-square variation in SNR^2), then the GNEQ and spatially averaged SNR^2 can be considered a useful summary of the efficacy of the detector.

In this paper we have applied the concept of an ideal observer directly to the digital data. The results obtained are

implicit in the work of Giger et al.,[13,25,41,42] but Giger et al. concentrates on issues of display and models of human visual response to the displayed data. As these tasks are decoupled from image acquisition for digital systems, it is worth considering figures of merit for the data acquisition system independent of the display, as done here. The results of this section also follow as limiting cases of the work of Barrett et al.[1] Of particular note, Sec. V A[1] discusses a simple binning detector and obtains

$$\text{SNR}^2 = \sum_{m=1}^{M} \frac{\Delta \bar{g}_m^2}{\sigma_m^2}, \qquad (85)$$

where σ_m is the uncorrelated noise in the mth detector and $\Delta \bar{g}_m$ is the expected change in the data value at the mth detector which would be caused by the signal. This particular result can be obtained directly from first principles based on counting statistics in each detector element. In the stationary case, $\sigma_m = \sigma$ is a constant, so in Eq. (78) $W(\mathbf{f}) = \sigma^2 |A|$ and the numerator [using Eq. (38) and Parseval's identity] becomes $|A| \sum_{\mathbf{m}} |\Delta \langle D(\mathbf{r_m}) \rangle|^2$, again recovering the result [Eq. (85)] based on counting statistics for uncorrelated noise. It is worth noting that if one does not include the aliased terms in the numerator of Eq. (78) (perhaps on the grounds that aliased signals are not useful), the value of SNR^2 will be underestimated. The aliased response is part of the physical response of the detector, and in this case the aliased terms will add coherently in such a manner as to bring the calculated value of the SNR^2 up to the value in Eq. (85) obtained from counting statistics.

VII. MODEL DETECTORS

To give a feel for the implications of the above theory, the capabilities of detectors with reasonably realistic parameters will now be investigated. The modeling is somewhat simplistic, but sufficient to demonstrate several interesting properties, such as the dependence of SNR on the position of the object being imaged, and certain trade-offs inherent in such detectors, particularly those trade-offs related to the possible suppression of input spatial frequencies above the frequencies supported by the lattice. The incident x-ray fluence Φ has a white Wiener spectrum, $W_i(\mathbf{f}) = \Phi$. Among other simplifications, which will be discussed in more detail at the end of the section, we assume 100% of the x-rays interact. Each x-ray undergoes a stochastic amplification, characterized by an average of m secondary quanta per x-ray with $\sigma_m = \sqrt{m}$ for a Poisson process, and the secondary quanta undergo a stochastic scattering process, with a spread function P_s and transfer function T_s, before being "binned" by the detector elements. The result is an average of $m\Phi$ secondary quanta per unit area on the detector with a pre-sampled Wiener spectrum given by[43]

$$W_s(\mathbf{f}) = [m^2 W_i(\mathbf{f}) + \Phi \sigma_m^2 - m\Phi] |T_s(\mathbf{f})|^2 + m\Phi. \qquad (86)$$

For a square lattice with spacing L, binning can be considered as a deterministic convolution with rect functions representing the detector regions, so that with

$$T_b(\mathbf{f}) = \left(\frac{\sin(\pi L f_x)}{\pi L f_x} \right) \left(\frac{\sin(\pi L f_y)}{\pi L f_x} \right), \qquad (87)$$

the digital noise power spectrum can be written

$$W(\mathbf{f}) = \frac{1}{m^2} \sum_{\mathbf{f_k}} |A|^2 \Phi(m^2 |T_s(\mathbf{f}+\mathbf{f_k})|^2 + m) |T_b(\mathbf{f}+\mathbf{f_k})|^2 + W_E, \qquad (88)$$

where the factor of $1/m^2$ is introduced so that digital values will correspond to x-ray count and W_E is the electronic noise. With the present conventions the gray-scale characteristic is set to $\Gamma = |A|$. A simplification can be achieved[44] using

$$\sum_{n=-\infty}^{\infty} \left(\frac{\sin(\pi(x+n))}{\pi(x+n)} \right)^2 = 1 \qquad (89)$$

for any x, which can be proven by applying Parseval's theorem to the Fourier series for $e^{2\pi i x y}$ for $y \in [-0.5, 0.5]$. The experimentally observable transfer function (as obtained, for example, by the slanted-edge technique, cf. Sec. IV) contains the effects of stochastic scatter and binning, thus $T(\mathbf{f}) = T_s(\mathbf{f}) T_b(\mathbf{f})$, so that

$$W(\mathbf{f})/|A| = \Phi |A| \sum_{\mathbf{f_k}} |T(\mathbf{f}+\mathbf{f_k})|^2 + \frac{\Phi |A|}{m} + W_E/|A| \qquad (90)$$

is the Wiener spectrum of the model detector, with the average number of x-rays per pixel being $\Phi |A|$. The summation over aliases in Eq. (88) is often referred to as "noise aliasing." The division into aliased and unaliased components is useful for modeling a variety of detectors, but it should be noted that this division is generally not directly experimentally accessible, at least not without modifying the detectors, and that in principle there could be devices which are stationary, and therefore have Wiener spectra, but for which the division of the NPS into aliased and unaliased components is not useful.

It is useful to choose values of the parameters in the model which are representative of detectors of current clinical interest, as this can help in the understanding of the physics which determines the performance of these devices, but detailed modeling for quantitative comparison to actual devices is beyond the scope of this article. We assume a square lattice with spacing of $L = 0.143$ mm, operation at an exposure corresponding to $|A|\Phi = 1400$ x-rays per pixel, and an amplification factor of $m = 1000$. For the stochastic transfer function T_s we consider three possibilities: a "blur-free" detector for which $T_s(\mathbf{f}) = 1$, typical of photoconductive arrays,[45] and two "alias-free" detectors whose stochastic transfer functions are of the form $T_s(\mathbf{f}) = e^{-\lambda |\mathbf{f}|}$ with $\lambda = 0.463$ and $\lambda = 0.34$ mm, which approximates the transfer function for evaporated CsI.[46–48] Typically electronic noise $\sqrt{(W_E)/|A|}$ is on the order of 3–5 x-rays, so values of 0, 4^2, and 8^2 cover the range of values for $\Phi |A|/m + W_E/|A|$.

The transfer functions for these models are shown in Fig. 2. As the pixels are symmetric with respect to inversion through their centers [i.e., for the PSF, $P(\mathbf{r}) = P(-\mathbf{r})$, and
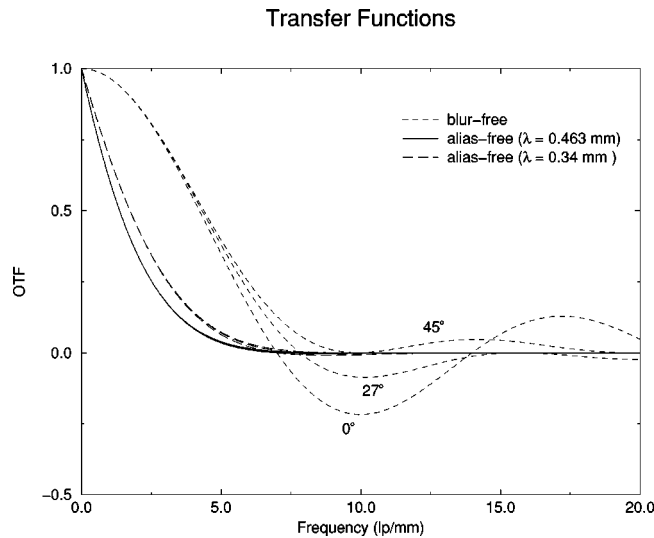
Transfer Functions

FIG. 2. The optical transfer functions of three model detectors. The ''blur-free'' detector bins the secondary quanta without smoothing, while for the ''alias-free'' detectors the distribution of secondary quanta is smoothed by an exponential MTF ($e^{-\lambda|\mathbf{f}|}$) before binning. Data are shown as a function of the magnitude of the spatial frequency for several angles.

GDQE

FIG. 4. GDQE as a function of frequency for the three model detectors as in Fig. 2, with the residual white noise $\Phi|A|/m + W_E/|A|$ set to 0.

$P(\mathbf{r})$ is a real number], the imaginary part of the transfer function is identically zero, so only the real part need be graphed. The OTF is, of course, a function of two variables, f_x and f_y. To show this, we plot the OTF as a function of the magnitude of the frequency vector for three angles relative to an axis of the detector. For the blur-free detector, the transfer function is simply the product of the sincs in the two directions induced by the binning operation. The OTF of the blur-free detector is nonzero well beyond the highest frequency supported by the lattice. Any component of an input signal at these higher frequencies will contribute to a lower frequency alias in the output, as per Eq. (38), and while it is not obvious from the point of view of frequency space the sum over aliases in Eq. (38) will be precisely equivalent to the detector
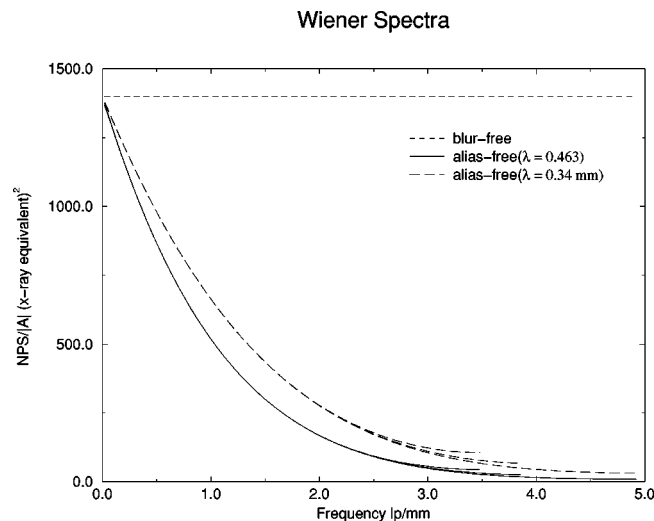
Wiener Spectra

FIG. 3. The Wiener spectra $W(\mathbf{f})/|A|$ for the three model detectors as in Fig. 2. The residual additive white noise $\Phi|A|/m + W_E/|A|$ has been set to 0.
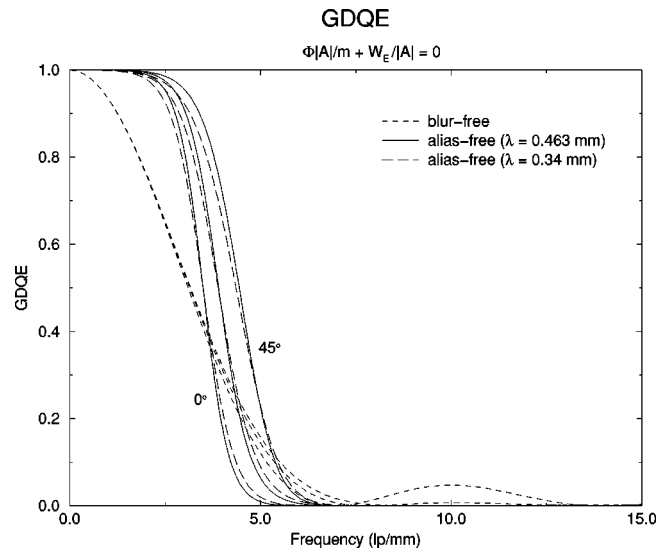
simply binning each incident x-ray. For the alias-free detectors, there is very little response to frequencies beyond those supported by the lattice. For each detector, three angles are plotted, but the angular dependence for the alias-free detectors is small enough to not be apparent on the graph.

The Wiener spectra are shown in Fig. 3. Again, instead of plotting a function of two variables, f_x and f_y, we plot the NPS as a function of the magnitude of the frequency vector for three angles, $\theta=0$, 27, and 45° (27° corresponds to a slope of 1:2 relative to the lattice). However, the NPS shows little angular dependence. For the Wiener spectrum one only needs to look at frequency values supported by the lattice, i.e., $f_x \in [-1/2L, 1/2L]$ and $f_y \in [-1/2L, 1/2L]$ (for convenience one can consider W to be periodic in the frequency plane). Thus, at $\theta=0°$ one only needs to graph up to $1/2L = 3.5\,\mathrm{mm}^{-1}$, but at $\theta=45°$ the frequencies are on the diagonal of the square, so one goes up to $\sqrt{2}/2L = 4.9\,\mathrm{mm}^{-1}$. At $\theta=27°$, one goes up to $1/(2L \cos\theta) = 4\,\mathrm{mm}^{-1}$. For this graph the constant offset $\Phi|A|/m + W_E/|A|$ has been set to zero. For the blur-free detector, the NPS is flat, which follows mathematically from Eq. (89) and the fact that $T(\mathbf{f})$ for these detectors is simply related to sinc functions, or more physically by noting that for a detector which simply bins incident x-rays adjacent cells will be uncorrelated so the NPS is flat. For the alias-free detectors, the NPS is suppressed by factors of the square of the transfer function.

The GDQE as a function of frequency are shown in Figs. 4–6 for a range of values of the residual white noise $\Phi|A|/m + W_E/|A|$. For each graph, values are plotted as a function of the magnitude of the spatial frequency for angles 0, 27, and 45° relative to an axis. In each case, the GDQE falls off most quickly at $\theta=0°$ and least quickly at $\theta=45°$, which represents the fact that on the diagonal the sampling rate is increased by a factor of $\sqrt{2}$. In the case where the residual white noise is zero (Fig. 4), the GDQE of the blur-free detector drops like the square of a sinc function. For the
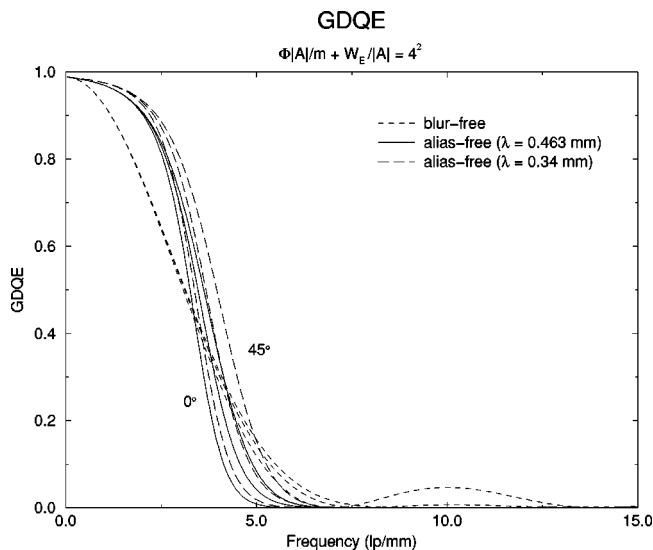
GDQE

$\Phi|A|/m + W_E/|A| = 4^2$

FIG. 5. GDQE as a function of frequency for the three model detectors as in Fig. 2, with the residual white noise $\Phi|A|/m + W_E/|A|$ set to 4^2.

alias-free detectors, the GDQE remains at nearly unity up to the lattice cutoff, the factor of $T^2(\mathbf{f})$ canceling the same factor in the colored part of the noise. The GDQE of the blur-free detector shows some response beyond the lattice cutoff. Though small, this portion of the GDQE is physical and it will be shown that the responses to the aliased frequencies can not be trivially dismissed. With the addition of residual white noise the GDQE of all three models is reduced, as shown in Fig. 5 ($\Phi|A|/m + W_E/|A| = 4^2$) and Fig. 6 ($\Phi|A|/m + W_E/|A| = 8^2$). These figures illustrate that the alias-free detectors are more sensitive to sources of residual white noise than blur-free detectors. Indeed, in Fig. 6 the blur-free detector now has higher GDQE than the $\lambda = 0.463$ mm detector even at low spatial frequencies. From the spatial point of view this is quite reasonable. A detector
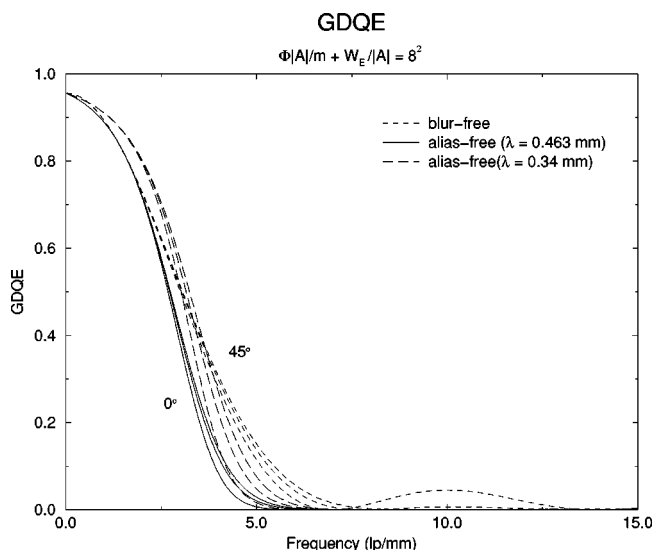
GDQE

$\Phi|A|/m + W_E/|A| = 8^2$

FIG. 6. GDQE as a function of frequency for the three model detectors as in Fig. 2, with the residual white noise $\Phi|A|/m + W_E/|A|$ set to 8^2.
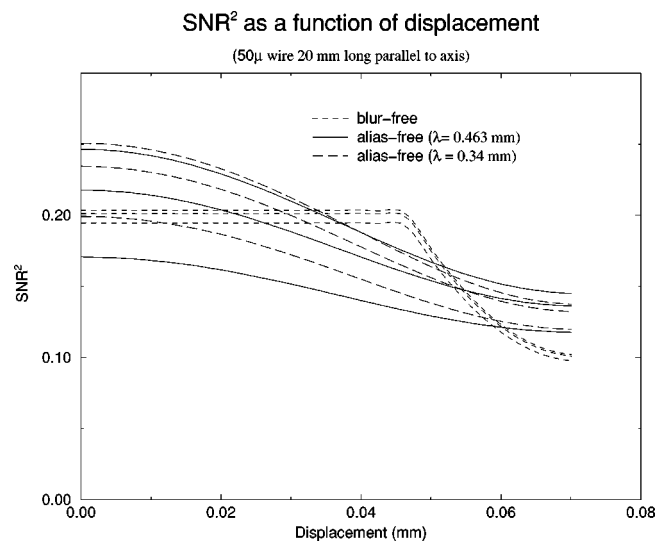
SNR^2 as a function of displacement

(50μ wire 20 mm long parallel to axis)

FIG. 7. Relative SNR^2 as a function of position for a 50 μm wide, 20 mm long wirelike object parallel to one axis of the detector. The horizontal axis of the graph gives the displacement of the wire, so that at 0 mm the wire is over a single column of sensitive elements, while at 0.07 mm the wire straddles two columns. The verticle scale is arbitrary (dependent upon the contrast of the wire).

whose transfer function is designed to remove aliases has a relatively wide point spread function, and therefore a relatively wide autocovariance function. The ideal observer makes use of digital values in array elements whose distance from the position of the signal is up to several times the lengths of the tails of these functions, so for the same input signal the ideal observer will have to integrate over a larger region on an alias-free detector and thus will be more sensitive to any residual uncolored noise.

While GDQE is directly related to the average value of SNR^2 by Eq. (82), high-frequency signals (i.e., x-ray projection images of small objects or objects whose projected density varies quickly with position) can demonstrate significant changes in SNR^2 with position. To explore this, consider the SKE/BKE task associated with an object 50 μm wide and 20 mm long. Wires of this width have been used in neurological and cardiovascular stents.[49] Figure 7 shows the SNR^2 for such an object, oriented parallel to an axis of the detector, as a function of displacement in the direction of the shorter (50 μm) axis. The scale of the vertical axis is arbitrary as we won't set the inherent contrast of the signal. In Fig. 7, the 0 mm displacement corresponds to the signal being centered over the sensitive elements of the detectors. For the blur-free detector, at 0 mm displacement the signal falls into a single column of detectors, so the SNR^2 corresponds to counting statistics for one column of elements 20 mm long. The SNR^2 is constant until the 0.05 mm mark, after which the signal is shared between two columns of detectors, resulting in a drop in SNR^2. Physically, the number of x-rays attenuated by the object is independent of its position, but at a displacement of 0.7 mm the signal is shared equally between two columns, and since the noise is assumed to be uncorrelated, the variance in the total counts in the two columns is twice that of one column, so the SNR^2 is

TABLE I. SNR^2 averaged over position and orientation for the projection image of an object 0.05 by 20 mm. As the SNR^2 scales with the square of the contrast of the image, only relative values are meaningful. The ± represent the rms (root-mean-square) fluctuations in the SNR^2 with position, not the statistical uncertainties.

	SNR^2 for 50 μm wide, 20 mm long object		
	$\Phi|A|/m + W_E/|A| = 0$	$= 4^2$	$= 8^2$
Blur-free	1.81±0.02	1.79±0.02	1.73±0.02
Alias-free (λ=0.463 mm)	2.16±0.16	1.87±0.07	1.48±0.02
Alias-free (λ=0.34 mm)	2.15±0.15	1.99±0.10	1.68±0.05

TABLE III. SNR^2 averaged over position and orientation for detecting the projection of a 0.5 mm square. Normalization is arbitrary. The ± represents the rms fluctuations in the SNR^2 with position, not the statistical uncertainties.

	SNR^2 for 0.5 mm square		
	$\Phi|A|/m + W_E/|A| = 0$	$= 4^2$	$= 8^2$
Blur-free	1.91±0.01	1.89±0.01	1.83±0.01
Alias-free (λ=0.463 mm)	2.08±0.01	1.99±0.01	1.789±0.003
Alias-free (λ=0.34 mm)	2.07±0.01	2.01±0.01	1.855±0.006

reduced by half. The alias-free detectors show less sensitivity to position, as the signal is always shared between multiple columns. As before, curves are shown for three values of the residual white noise $\Phi|A|/m + W_E/|A|(0^2, 4^2,$ and $8^2)$. For all models, the SNR^2 drops as the residual white noise increases, but this effect is greater for the alias-free models. Table I gives the average SNR^2 for detection of the 0.05 wide, 20 mm long wire, now averaged over both position and orientation. Additionally, the root-mean-square variation in SNR^2 is given, to indicate the degree to which the detectability of the wire would vary. Again, the alias-free detectors give a higher SNR^2 if the residual white noise is kept sufficiently low. In calculating the SNR^2 of the projection of the wire using Eq. (78), if the summation over aliases is dropped, the resulting integral decreases by about 10%. Thus the contributions of the aliased signal to the SNR are not always negligible.

Somewhat speculatively one can consider tasks which depend upon higher frequency components of the signal.[50] Consider a 5 mm square with 10% contrast, and a second square whose edges have been smoothed by convolving with a 0.15 mm rect function, so that the resulting signal ''ramps up'' over a distance of 0.3 mm. The SNR^2 for the SKE/BKE task of distinguishing between these two objects is given in Table II. It is interesting to note that, mathematically, the SNR^2 is sufficiently large that the ideal observer can perform this task efficiently, although whether a human could do this is questionable. On the other hand, edge detection is important both computationally and probably as part of the strategy of human observers, so the ability to perform this task is not *a priori* irrelevant. Again, the alias-free detectors have a higher SNR^2 if the residual white noise is zero, but as the task now depends more heavily on the higher frequency

components of the signal, the alias-free detectors are more sensitive to residual white noise, with the crossover at $\Phi|A|/m + W_E/|A| = 4^2$. The detection of a 0.5 mm square is shown in Table III. Here, the lower (but nonzero) frequencies dominate the response of the detector, so that in general the antialiasing detectors gain from the removal of the aliased noise without losing any signal.

It is interesting to note that the SNRs for the tasks and models described above do not vary greatly. Many factors not considered here will greatly effect the performance of real detectors, beginning with the fact that less than 100% of the incident x-rays will produce secondary quanta. The color of the Wiener spectrum need not be the same as the transfer function, due to, for example, x-rays interacting at various depths in the detector.[51] The efficiency of collection of the secondary quanta can also have significant effects.[52] For CsI detectors, of which our ''alias-free'' detector is a rough model, the fill factor is a minor effect so long as the amplification m is sufficiently large.[48] For selenium detectors, of which our ''blur-free'' detector is an approximation, it is possible to have an effective fill factor significantly greater than the geometric fill factor of the TFT array.[53,54] In any case, our purpose here is merely to indicate some of the issues which must be faced in quantifying digital detectors of these types. In addition, we did not consider geometric factors such as x-ray focal spot size and x-ray parallax[48] which reduce the high-frequency content of the incoming signals.

VIII. DISCUSSION AND CONCLUSION

The results of this paper set up a framework for quantitative measurements of digital systems in a manner analogous to the now common analysis of screen-film systems in terms of the gray-scale transfer characteristic, the optical transfer function, the Wiener spectrum, and signal-to-noise ratio. The logic of this framework is by design close to the classic work on film-screen systems. While many pieces of this argument have appeared in the work of others, as noted throughout the text, it seemed desirable to produce a coherent systematic exposition. The results can be seen as appropriate limits of those of Barrett *et al.*, but the theoretical construction here emphasizes the parallels with the classic results on screen-film systems. While detectors consisting of discrete elements do not have continuous translational symmetry, the remaining discrete symmetry allows one to use the appropriate Fourier technique. The advantage of this, as in the screen-film

TABLE II. SNR^2 averaged over position and orientation for distinguishing between the projection of a 5 mm square with sharp boundaries and a square whose boundaries ramp up over a 0.3 mm region. Normalization corresponds to a 10% contrast with an x-ray flux corresponding to 1400 x-rays/pixel. The ± represents the rms fluctuations in the SNR^2 with position, not the statistical uncertainties.

	SNR^2 for discontinuity vs slope		
	$\Phi|A|/m + W_E/|A| = 0$	$= 4^2$	$= 8^2$
Blur-free	14±2	14±2	13±2
Alias-free (λ=0.463 mm)	16±3	12±1	7.6±0.5
Alias-free (λ=0.34 mm)	16±3	14±2	10±1

case, is that one can explicitly solve for the mask function of the ideal observer [see Eq. (75)] and thereby obtain the optimal SNR. As for screen-film, this formula can be interpreted as the ratio of the square of the signal in each frequency bin to the noise in each frequency bin, as measured by the Wiener spectrum, integrated over bins.

We have investigated several highly idealized, but not completely unrealistic, models of detectors, and illustrated some of the issues inherent in various design decisions. This analysis is incomplete and intended to point toward issues which could be addressed in other work. However, our results suggest that for typical tasks the detectability of objects as determined by SNR^2 is not drastically affected by the decision, in and of itself, to suppress or not to suppress aliases. In any real device, of course, this design decision is linked to many other parameters. This article should be of use in clarifying what is actually experimentally measured in testing such devices.

The results presented here are exact for the SKE/BKE task as approached by the ideal observer under the assumptions of linearity, homogeneity, and stationarity. However, each of these assumptions is only approximately true in practice. The finite extent of real detectors trivially shows that they are not homogeneous, but for a variety of tasks edge effects are negligible. More importantly, many digital detectors in practice show significant inhomogeneity and nonstationarity. The work of Barrett et al. is sufficiently general to cover these cases. Further, the inhomogeneity and nonstationarity of a given instrument often occur in ways which are different for each individual device, so that while the extra information is relevant to the particular device one has measured, the extra information is often not generalizable to other devices of the same manufacture. This extra information is useful for optimizing certain tasks using the particular device, but less use in understanding a class of devices. Additionally, while the signal detection task of the ideal observer under SKE/BKE conditions certainly shares some features with the task which human observers face, and has under many conditions been shown to correlate well with the ability of human observers (for example, screen-film images of nylon beads[55]), it is still a very idealized task. For example, if edge-detection is important, then higher frequency parts of the incoming signal become more important than would be expected given simply the signal detection task. From the point of view of a radiologist, a clear edge might be used to identify and distinguish the existence of a lesion from a variation in projected density of the underlying organ, particularly in the presence of the ''structured noise'' of other anatomical features.

Clearly these are issues for further study, but while OTF, W, SNR, and GDQE are certainly useful because they are objectively measurable and in a mathematically precise manner are related to tasks which approximate those of the human observer, it is worth remembering that measurement of these quantities does not obviate the need for observer studies, particularly with practicing radiologists.

[a] Author to whom correspondence should be addressed; electronic mail: Andrew.Maidment@mail.tju.edu

[1] H. H. Barrett, J. L. Denny, R. F. Wagner, and K. J. Myers, ''Objective assessment of image quality. II. Fisher information, Fourier crosstalk, and figures of merit for task performance,'' J. Opt. Soc. Am. A **12**(5), 834–852 (1995).

[2] H. H. Barrett and H. C. Gifford, ''Cone-beam tomography with discrete data sets,'' Phys. Med. Biol. **39**, 451–476 (1994).

[3] J. M. Boone, ''X-ray imaging concepts: Mathematics and modeling,'' in *Specification, Acceptance Testing and Quality Control of Diagnostic X-ray Imaging Equipment*, edited by J. A. Seibert, G. T. Barnes, and R. G. Gould, Medical Physics Monograph (AIP, Woodbury, NY, 1994), pp. 75–107.

[4] M. J. Yaffe and R. M. Nishikawa, ''X-ray imaging concepts: Noise, SNR and DQE,'' in *Specification, Acceptance Testing and Quality Control of Diagnostic X-ray Imaging Equipment*, edited by J. A. Seibert, G. T. Barnes, and R. G. Gould, Medical Physics Monograph (AIP, Woodbury, NY, 1994), pp. 109–144.

[5] J. C. Dainty and R. Shaw, *Image Science* (Academic, New York, 1974).

[6] H. H. Barrett and W. Swindell, *Radiological Imaging* (Academic, New York, 1981).

[7] ICRU, ''Medical imaging—The assessment of image quality,'' Technical Report No. 54, International Commission on Radiation Units and Measurements, Bethesda, Maryland, 1996.

[8] R. S. Strichartz, *A Guide to Distribution Theory and Fourier Transforms* (CRC, Boca Raton, 1994).

[9] H. L. van Trees, *Detection, Estimation, and Modulation Theory (Part I)* (Wiley, New York, 1968).

[10] J. B. Thomas, *An Introduction to Statistical Communication Theory* (Wiley, New York, 1969).

[11] R. F. Wagner and D. G. Brown, ''Unified SNR analysis of medical imaging systems,'' Phys. Med. Biol. **30**, 489–518 (1985).

[12] A. V. Oppenheim, R. W. Schafer, and J. R. Buck, *Discrete-Time Signal Processing*, 2nd ed. (Prentice Hall, Upper Saddle River, NJ, 1999).

[13] M. L. Giger, K. Doi, and C. E. Metz, ''Investigation of basic imaging properties in digital radiography. II. Noise Wiener spectrum,'' Med. Phys. **11**, 797–805 (1984).

[14] J. W. Cooley, P. A. W. Lewis, and P. D. Welch, *The Fast Fourier Transform Algorithm and Its Applications, RC-1743* (IBM Watson Research Center, Yorktown Heights, NY, 1967).

[15] A. Papoulis, *Probability, Random Variables, and Stochastic Processes*, 3rd ed. (McGraw-Hill, New York, 1991).

[16] G. B. Folland, *Fourier Analysis and its Applications* (Brooks/Cole, Pacific Grove, CA, 1992).

[17] J. J. Benedetto, *Harmonic Analysis and Applications* (CRC, Boca Raton, 1997).

[18] F. O. Huck, N. Halyo, and S. K. Park, ''Aliasing and blurring in 2-D sampled imagery,'' Appl. Opt. **19**, 2174–2181 (1980).

[19] S. K. Park, R. Schowengerdt, and M.-A. Kaczynski, ''Modulation-transfer-function analysis for sampled image systems,'' Appl. Opt. **23**, 2572–2582 (1984).

[20] P. F. Judy, ''The line spread function and modulation transfer function of a computed tomographic scanner,'' Med. Phys. **3**, 233–236 (1976).

[21] S. E. Reichenbach, S. K. Park, and R. Narayanswamy, ''Characterizing digital image acquisition devices,'' Opt. Eng. **30**, 170–177 (1991).

[22] I. A. Cunningham and A. Fenster, ''A method for modulation transfer function determination from edge profiles with correction for finite-element differentiation,'' Med. Phys. **14**, 533–537 (1987).

[23] H. Fujita et al., ''A simple method for determining the modulation transfer function in digital radiography,'' IEEE Trans. Med. Imaging **11**, 34–39 (1992).

[24] J. T. Dobbins III, ''Effects of undersampling on the proper interpretation of modulation transfer function, noise power spectra, and noise equivalent quanta of digital imaging system,'' Med. Phys. **22**, 171–181 (1995).

[25] M. L. Giger and K. Doi, ''Investigation of basic imaging properties in digital radiography. I. Modulation transfer function,'' Med. Phys. **11**, 287–295 (1984).

[26] C. E. Metz, ''Basic imaging theory,'' in *Recent Developments in Digital Imaging* (1984 Summer School), edited by K. Doi *et al.*, Medical Physics Monograph (AIP, New York, 1985), pp. 1–15.

[27] R. A. Sones and G. T. Barnes, ''A method to measure the MTF of digital x-ray systems,'' Med. Phys. **11**, 166–171 (1984).

[28] H. Fujita, K. Doi, and M. L. Giger, ''Investigation of basic imaging properties in digital radiography. 6. MTFs of II-TV digital imaging systems,'' Med. Phys. **12**, 713–720 (1985).

[29] F. J. Harris, ''On the use of windows for harmonic analysis with the discrete Fourier transform,'' Proc. IEEE **66**, 51–83 (1978).

[30] R. F. Wagner and J. M. Sandrik, ''An introduction to digital noise analysis,'' in *The Physics of Medical Imaging: Recording System Measurements and Techniques* (1979 Summer School), edited by A. G. Haus, Medical Physics Mongograph (AIP, New York, 1979), pp. 524–545.

[31] I. A. Cunningham, ''Analyzing system performance,'' in *The Expanding Role of Medical Physics in Diagnostic Imaging*, Proceedings of the 1997 Summer School, edited by G. D. Frey and P. Sprawls (Advanced Medical Publishing, Madison, Wisconsin, 1997), pp. 231–263.

[32] I. A. Cunningham, in *Handbook of Medical Imaging*, edited by J. Beutel, H. L. Kundel, and R. L. van Metter (SPIE, Bellingham, WA, 2000), Vol. 1, Chap. 2.

[33] W. A. Gardner and L. E. Franks, ''Characterization of cyclostationary random signal processes,'' IEEE Trans. Inf. Theory **IT-21**, 4–14 (1975).

[34] J. S. Bendat and A. G. Piersol, *Random Data* (Wiley, New York, 1986).

[35] H. H. Barrett and C. K. Abbey, in Lecture Notes in Computer Science, edited by J. Duncan and G. Gindi (Springer, Berlin, 1997), Vol. 1230, pp. 155–166.

[36] H. H. Barrett, C. K. Abbey, and E. Clarkson, ''Objective assessment of image quality. III. ROC metrics, ideal observers, and likelihood-generating functions,'' J. Opt. Soc. Am. A **15**(6), 1520–1535 (1998).

[37] D. M. Green and J. A. Swets, *Signal Detection Theory and Psychophysics* (Wiley, New York, 1966).

[38] I. Karatzas and S. E. Shreve, *Brownian Motion and Stochastic Calculus*, 2nd ed. (Springer, New York, 1991).

[39] E. Clarkson and H. Barrett, in *Lecture Notes in Computer Science*, edited by J. Duncan and G. Gindi (Springer, New York, 1997), Vol. 1230, pp. 549–554.

[40] D. G. Brown, M. F. Insana, and M. Tapiovaara, ''Detection performance of the ideal decision function and its McLaurin expansion: Signal position unknown,'' J. Acoust. Soc. Am. **97**, 379–398 (1995).

[41] M. L. Giger and K. Doi, ''Effect of pixel size on detectability of low-contrast signals in digital radiography,'' J. Opt. Soc. Am. A **4**(5), 966–975 (1987).

[42] M. L. Giger and K. Doi, ''Investigation of basic imaging properties in digital radiography, 3. Effect of pixel size on SNR and threshold contrast,'' Med. Phys. **12**, 201–208 (1985).

[43] M. Rabbani, R. Shaw, and R. van Metter, ''Detective quantum efficiency of imaging systems with amplifying and scattering mechanisms,'' J. Opt. Soc. Am. A **4**(5), 895–901 (1987).

[44] K. M. Hanson, ''The detective quantum efficiency of CT reconstruction: The detection of small objects,'' in *Application of Optical Instruments in Medicine VII*, edited by J. E. Gray, Proc. SPIE **173**, 291–298 (1979).

[45] D. L. Lee, L. K. Cheung, B. Rodricks, and G. F. Powell, ''Improved imaging performance of a 14×17-inch Direct Radiolgraphy (TM) System using Se/TFT detector,'' in *SPIE Conference on Physics of Medical Imaging* [Proc. SPIE **3336**, 14–23 (1998)].

[46] J.-P. Moy, ''Image quality of scintillator based X-ray electronic imagers,'' in *SPIE Conference on Physics of Medical Imaging* [Proc. SPIE **3336**, 187–194 (1998)].

[47] C. Chaussat, J. Chabbal, T. Ducourant, V. Spinnler, G. Vieux, and R. Neyret, ''New CsI/a-Si 17″×17″ X-ray flat panel detector provides superior detectivity and immediate direct digital output for General Radiography systems,'' in *SPIE Conference on Physics of Medical Imaging* [Proc. SPIE **3336**, 45–55 (1998)].

[48] J.-P. Moy, ''Signal-to-noise ratio and spatial resolution in x-ray electronic imagers: Is the MTF a relevant parameter?,'' Med. Phys. **27**, 86–93 (2000).

[49] J. J. Connors III, J. C. Wojak, and Z. Qian, in *Interventional Neuroradiology: Strategies and Practical Techniques*, edited by J. J. Connors III, and J. C. Wojak (W. B. Saunders, Philadelphia, 1999), Chap. 1.

[50] K. M. Hanson, ''Variations in task and the ideal observer,'' Proc. SPIE **419**, 60–67 (1983).

[51] G. Lubberts, ''Random noise produced by x-ray fluorescent screens,'' J. Opt. Soc. Am. **58**, 1475–1483 (1968).

[52] I. A. Cunningham, ''Degradation of the detective quantum efficiency due to a non-unity detector fill factor,'' in Phys. Med. Imaging **3032**, 22–31 (1997).

[53] J. A. Rowlands and J. Yorkston, in *Handbook of Medical Imaging*, edited by J. Beutel, H. L. Kundel, and R. L. van Metter (SPIE, Bellingham, WA, 2000), Vol. 1, Chap. 4.

[54] G. Pang, W. Zhao, and J. A. Rowlands, ''Digital radiology using active matrix readout of amorphous selenium: Geometrical and effective fill factors,'' Med. Phys. **25**, 1636–1646 (1998).

[55] L.-N. D. Loo, K. Doi, and C. E. Metz, ''A comparison of physical image quality indices and observer performance in the radiographic detection of nylon beads,'' Phys. Med. Biol. **29**, 837–856 (1984).